AFOSR-TR. 81-0584

(14)

AD A102030

AAE

AERONAUTICAL
AND ASTRONAUTICAL
ENGINEERING DEPARTMENT

DTIC
ELECTE
JUL 2 4 1981

ENGINEERING EXPERIMENT STATION, COLLEGE OF ENGINEERING, UNIVERSITY OF ILLINOIS, URBANA

81 7 22 105

Aeronautical and Astronautical Engineering Department

University of Illinois at Urbana-Champaign

Technical Report AAE-81-1

UILU-Eng-81-0501

Prepared for

SHOCK DEVELOPMENT AND TRANSITION

TO DETONATION INITIATED BY BURNING IN

POROUS PROPELLANT BEDS

by

P. Barry Butler and Herman Krier

Conditions of Reproduction

JUL 2 4 1981

REPORT DOCUMENTATION PAGE	READ INSTRUCTIONS BEFORE COMPLETING FORM

1. REPORT NUMBER	2. GOVT ACCESSION NO.	3. RECIPIENT'S CATALOG NUMBER
AFOSR-TR- 81 -0584	AD-A102030	

4. TITLE (and Subtitle)	5. TYPE OF REPORT & PERIOD COVERED
"SHOCK DEVELOPMENT AND TRANSITION TO DETONATION INITIATED BY BURNING IN POROUS PROPELLANT BEDS"	INTERIM FEBRUARY 1981
	6. PERFORMING ORG. REPORT NUMBER

7. AUTHOR(s)	8. CONTRACT OR GRANT NUMBER(s)
P B BUTLER H KRIER	AFOSR-77-3336

9. PERFORMING ORGANIZATION NAME AND ADDRESS	10. PROGRAM ELEMENT, PROJECT, TASK AREA & WORK UNIT NUMBERS
UNIVERSITY OF ILLINOIS URBANA, IL 61801	2308/A2 61102F

11. CONTROLLING OFFICE NAME AND ADDRESS	12. REPORT DATE
AIR FORCE OFFICE OF SCIENTIFIC RESEARCH/NA BUILDING 410	FEBRUARY 1981
	13. NUMBER OF PAGES
BOLLING AFB, DC 20332	103

14. MONITORING AGENCY NAME & ADDRESS(if different from Controlling Office)	15. SECURITY CLASS. (of this report)
	UNCLASSIFIED
	15a. DECLASSIFICATION DOWNGRADING SCHEDULE

16. DISTRIBUTION STATEMENT (of this Report)

Approved for public release; distribution unlimited.

17. DISTRIBUTION STATEMENT (of the abstract entered in Block 20, if different from Report)

18. SUPPLEMENTARY NOTES

19. KEY WORDS (Continue on reverse side if necessary and identify by block number)

DEFLAGRATION TO DETONATION TRANSITION
GRANULAR EXPLOSIVES
PROPELLANTS
PACKED BEDS

20. ABSTRACT (Continue on reverse side if necessary and identify by block number)

This report summarizes the analyses of deflagration to detonation transition (DDT) occurring in a packed bed of granular, high energy solid propellant. A reactive two-phase flow model of this phenomena is solved by utilizing a Lax-Wendroff finite differencing technique. A brief overview of the well-known shock jump conditions for one-dimensional, one-phase flow with heat addition is reported, and a similar analysis for one-dimensional, two phase reactive flow is discussed. Improvements made in the gas phase nonideal

DD FORM 1473 EDITION OF 1 NOV 65 IS OBSOLETE
1 JAN 73

UNCLASSIFIED

equation of state, gas permeability, and numerical integration techniques allow for the prediction of a transition to a steady detonation from initiation by deflagration. Analyses are presented that clearly indicate the effect of the propellant physical and chemical parameters on the predicted run-up length to detonation. Predictions of this run-up length to detonation are presented as a function of propellant chemical energy, burning rate, bed porosity, and granulation (size). Limited comparison with actual DDT data in the literature indicates good qualitative agreement with these predictions.

ABSTRACT

This report summarizes the analyses of deflagration to detonation transition (DDT) occurring in a packed bed of granular, high energy solid propellant. A reactive two-phase flow model of this phenomena is solved by utilizing a Lax-Wendroff finite differencing technique. A brief overview of the well known shock jump conditions for one-dimensional, one-phase flow with heat addition is reported, and a similar analysis for one-dimensional, two-phase reactive flow is discussed. Improvements made in the gas phase nonideal equation of state, gas permeability, and numerical integration t chniques allow for the prediction of a transition to a steady detonation from initiation by deflagration.

Analyses are presented that clearly indicate the effect of the propellant physical and chemical parameters on the predicted run-up length to detonation. Predictions of this run-up length to detonation are presented as a function of propellant chemical energy, burning rate, bed porosity, and granulation (size). Limited comparison with actual DDT data in the literature indicates good qualitative agreement with these predictions.

TABLE OF CONTENTS

iv

v

LIST OF FIGURES

LIST OF SYMBOLS

Notation	Definition	Units English	SI
a	Local Sound Speed	in/s	m/s
$\underline{b}$	Burning Rate Proportionality Constant	$\dfrac{\text{in/s}}{(\text{psi})^n}$	$\dfrac{\text{m/s}}{(N/m^2)^n}$
b	Nonideal Equation of State Constant	$\dfrac{lb_m}{in^3}$	$\dfrac{kg}{m^3}$
c	Nonideal Equation of State Constant	$\dfrac{lb_m^2}{in^6}$	$\dfrac{kg^2}{m^6}$
C_p	Specific Heat at Constant Pressure	$\dfrac{BTU}{lb_m\text{-}^\circ R}$	$\dfrac{J}{kg\text{-}^\circ K}$
C_v	Specific Heat at Constant Volume	$\dfrac{BTU}{lb_m\text{-}^\circ R}$	$\dfrac{J}{kg\text{-}^\circ K}$
D	Detonation Velocity	in/s	m/s
$\underline{c}$	Mixture Sound Speed	in/s	m/s
$\mathcal{D}$	Drag per Unit Volume on Particle	$\dfrac{lb_f}{in^3}$	$\dfrac{N}{m^3}$
d_p	Particle Diameter	in	m
E_{CHEM}	Chemical Energy	$\dfrac{BTU}{lb_m}$	$\dfrac{J}{kg}$
E_T	Total Energy	$\dfrac{BTU}{lb_m}$	$\dfrac{J}{kg}$
E_{int}	Internal Energy	$\dfrac{BTU}{lb_m}$	$\dfrac{J}{kg}$
E_{ign}	Ignition Energy	$\dfrac{BTU}{lb}$	$\dfrac{J}{kg}$
f_{pg}	Interphase Drag Coefficient	- - -	- - -
h_{pg}	Heat Transfer Coefficient	$\dfrac{BTU}{in^2\text{-s-}^\circ R}$	$\dfrac{J}{m^2\text{-s-}^\circ K}$
I	Number of Grid Points	- - -	- - -
K	Bulk Modulus	$\dfrac{lb_f}{in^2}$	$\dfrac{N}{m^2}$

k_g	Thermal Conductivity	$\dfrac{BTU}{in\text{-}S\text{-}^\circ R}$	$\dfrac{J}{m\text{-}s\text{-}^\circ K}$
ℓ_{cJ}	Run-Up Length to Detonation	in	m
L	Bed Length	in	m
M	Mach Number	---	---
N	Molecular Weight Reciprocol	$\dfrac{lb\text{-}mole}{lb}$	$\dfrac{kg\text{-}mole}{kg}$
$\underline{N}$	Number of Different Sized Particles	---	---
n	Burning Rate Index	---	---
$\underline{N}$	Number of Grid points in Bed	---	---
P	Gas Pressure	$\dfrac{lb_f}{in^2}$	$\dfrac{N}{m^2}$
P_p	Particle Stress	$\dfrac{lb_f}{in^2}$	$\dfrac{N}{m^2}$
Pr	Prandtl Number	---	---
$\dot{Q}$	Heat Transfer Rate per Unit Volume	$\dfrac{BTU}{in^3\text{-}s}$	$\dfrac{J}{m^3\text{-}s}$
R	Universal Gas Constant	$\dfrac{BTU}{lb_m\text{-}^\circ R}$	$\dfrac{J}{kg\text{-}^\circ K}$
r_p	Particle Radius	in	m
Re	Reynolds Number	---	---
$\dot{r}$	Burning Rate	$\dfrac{in}{s}$	$\dfrac{m}{s}$
t	Time	sec	sec
Δt	Time Increment	sec	sec
T	Temperature	$^\circ R$	$^\circ K$
u	Velocity	$\dfrac{in}{s}$	$\dfrac{m}{s}$
u_j	Product Velocity for CJ Detonation	in/s	m/s

V	Volume	---	---
X	Distance	in	m
β	Reaction Zone Thickness	in	m
γ	Isentropic Coefficient	---	---
γ_i	Ideal Limit of C_p/C_v	---	---
Γ	Mass Generation	$\dfrac{lb_m}{in^3-s}$	$\dfrac{kg}{m^3-s}$
λ	Coefficient in C.F.L. Stability Criteria	---	---
μ	Gas Viscosity	$\dfrac{lb_m}{in-s}$	$\dfrac{kg}{m-s}$
ν	Specific Volume	$\dfrac{in^3}{lb_m}$	$\dfrac{m^3}{kg}$
ρ	Density	$\dfrac{lb_m}{in^3}$	$\dfrac{kg}{m^3}$
ϕ	Porosity	---	---

Subscripts

atm	Atmospheric Conditions
A	Reactants
B	Products
CJ	Chapman-Jouget Condition
g	Gas
H	Hugoniot Curve
k	Location on Isentropic Expansion Wave Following Detonation
o	Initial Conditions
p	Particle
s	Isentropic
S	Strong Solution
w	Wall Condition
WK	Weak Solution
1	Gas Phase
2	Solid Phase

CHAPTER ONE

DEFLAGRATION-TO-DETONATION TRANSITION

1.1 Introduction

This report summarizes the analysis associated with the accelerating deflagration wave in a porous medium of reactive solid propellant. The phenomenon of DDT (deflagration-to-detonation transition) in solid propellants, especially solid propellants burning in rocket motor environments, is not usually considered a hazard. However, it may be that under certain situations, for example a grain structure failure, the solid motor may crack and form regions of granular or porous propellant. When flame from the surface deflagrating propellant reaches this seam of porous material it will accelerate into this medium and be supported by convective heat transfer from the burnt gas into the unignited porous region. If in addition to this the product gases are confined to a finite volume, the accelerating deflagration could transit into a detonation. Propellants exhibiting a high chemical energy per unit mass and capable of rapidly generating gases through their burning rate are more likely to experience this type of deflagration to detonation transition.

Analysis of the flows in such an unsteady two-phase mixture is a complicated exercise. Work has been underway at the University of Illinois since 1975 to develop a reactive hydrodynamic code in which the combustion of porous propellants can be modeled in such a way as to predict the behavior of a convectively driven flame in a confined situation. Details of these modeling exercises are found in References 1-4. In an evolutionary manner this work included the formulation of the two-phase flow conservation equations, first assuming that the mixture was a continuum, and at a

later date treating each phase as a separate continuum irrespective of the mixture properties. The most recent analysis of the unsteady two-phase flows associated with DDT is documented in the paper by Hoffman and Krier [3]. This reference, therefore, represents the starting point for the work that is presented here.

The reader, after reviewing the above noted reference, will understand that the modeling of this transient phenomena utilizes a number of important constitutive relations, which form closure of the conservation equations. For example, one must have information on the burning rate of the material that is a function of the surrounding pressure and temperature. One must also have laws for the dynamic gas permeability and the subsequent heat transfer rates of the hot gases as they are forced into the unignited porous material. In addition, relations which represent the resistance to compaction of the solid matrix must be included. Equations of state, not only for the high pressure in the product gases, but also for the solid itself, must be supplied (as shown in the work by Hoffman and Krier). The assumption of an incompressible solid, although providing some reasonable answers as far as the deflagration speed, is not an accurate indicator of the peak pressures that are possible during the accelerating deflagration mode. Since these pressures are precursor to the final detonation solutions that would be expected, it is clear that a compressible solid must be modeled.

In summary, the analysis of the DDT problem requires the solution of the conservation equations in both phases and the necessary constitutive relations. The conservation equations form a system of nonlinear hyperbolic equations, which require numerical finite differencing schemes. This report will summarize several of these integration schemes and will

evaluate which are more useful for this reactive flow problem. There are, of course, many numerical techniques available to handle hyperbolic partial differential equations which allow for solutions of shock waves. Obviously, not all of these have been treated in this work.

1.2 Previous Results on DDT Modeling

A review of References 2-4 indicates that a steady state detonation solution was not a predicted result. As will be shown in Sections 1.3 and 2.4, for propellant chemical energy, the initial solids loading considered and the material parameters (e.g. γ), a steady state detonation (CJ) would propagate at speeds of the order of 5-8 mm/μsec, with a detonation pressure of the order of 12-20 GPa. Although a fairly rapid flame front, often approaching a steady state speed of 2 mm/μsec was typical of the solutions presented in the work by Gokhale and Krier [2], Kezerle and Krier [4], and Hoffman and Krier [3], the associated peak pressures were never of significant manner to suggest that these final flame spreading rates were characteristic of an actual detonation, since fronts ranging from 1 to 2 mm/μsec cannot support a detonation (see following section). However, the peak pressures previously reported, which ranged between 1/2 to 5 GPa, were consistent with the velocities.

Continued work, which is reported here, indicates that it is now possible to obtain a detonation solution, but in order to do so a number of important modifications and corrections are required. To understand what these changes are and why they are necessary, it is appropriate at this point to first provide a review on the topic of detonation. Although the discussion that follows is documented in various manners in several textbooks, including such a review here will allow

for a clearer understanding of the steady state solution that is termed "detonation", as well as define the flow properties of the DDT analysis.

1.3 Jump Conditions for Reactive Flow

In order to understand the jump conditions across a detonation wave in two-phase (solid-gas) reactive flow, one should first look at the solution of the one-phase (all gas) flow problem. Fickett and Davis [5], and Strehlow [6] develop these jump equations in more detail in their texts. This section will give the reader a brief review of their work and highlight some of the key assumptions made in developing the Hugoniot and Rayleigh line equations.

In Figure 1 a detonation wave with velocity D is moving through a constant area duct into the unignited or "cold" end which is at rest. For this analysis all chemical reactions are assumed to take place in a narrow reaction zone. The products of combustion are shown moving with velocity u in the same direction as D. In this figure, the subscript A on pressure, density, and velocity designates the unignited or reactants side, and B indicates the product side of the combustion zone.

To better understand the jump conditions across the shock in Figure 1, a new frame of reference may be helpful. From a coordinate system attached to the moving detonation wave, an observer located at the origin would see the reactants moving with velocity $u_A = D$ into the stationary reaction zone and the products of combustion exiting with velocity $u_B = (D-u)$ (see Figure 2).

Conservation of mass and momentum through the flow area shown in Figure 2 gives respectively

$$\rho_A D = \rho_B u_B = \rho_B (D-u) \qquad (1)$$

Moving Reaction Zone

Reactants

P_A

ρ_A

$u_A = 0$

$\overset{D}{\longleftarrow}$ u $\longleftarrow$

Products

P_B

ρ_B

$u_B = u$
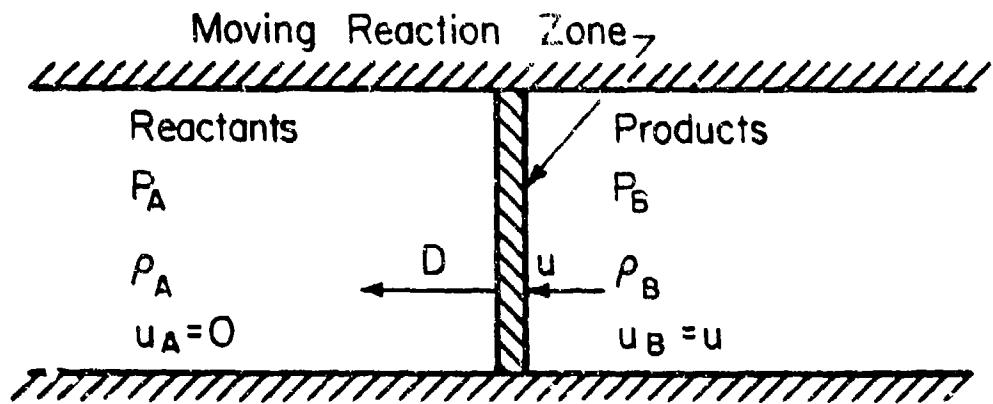
Fig. 1. Detonation Wave Moving into Stationary Reactants. (Reference Frame Fixed).

Stationary Reaction Zone

Reactants

P_A

$u_A = D$

ρ_A

$\longrightarrow$ $\longrightarrow$

Products

P_B

$u_B = D - u$

ρ_B
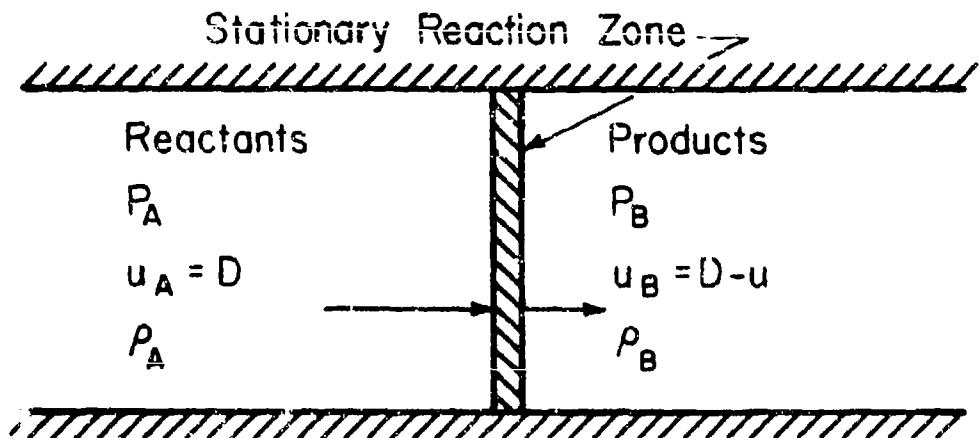
Fig. 2. Reactants Moving into Stationary Detonation Zone. (Reference Frame Moving with Reaction Zone).

and

$$\rho_A D^2 + P_A = \rho_B u_B^2 + P_B = \rho_B (D-u)^2 + P_B \tag{2}$$

In this model all viscous effects are confined within the bounds of the shock discontinuity. The expression for conservation of momentum (Eq. 2) can be simplified by making use of Equation 1 to obtain

$$P_B - P_A = \rho_A uD \tag{3}$$

Later, it will be assumed that P_A is nagligible with respect to P_B, but for the time P_A will be retained in the momentum equation.

Elimination of u, the reaction products velocity expressed in the fixed coordinate system, from Eqs. 1 and 3 gives the well known Rayleigh or Michelson line.

$$\rho_A^2 D^2 - (P_B - P_A)/(v_A - v_B) = 0 \tag{4}$$

Figure 3 illustrates a Rayleigh line on a P-v diagram for one specific value of D. The line has slope $-\rho_A^2 D^2$ and passes through the point (P_A, v_A). For the case where $D \to \infty$, the Rayleigh line approaches vertical and for $D \to 0$, the Rayleigh line is horizontal. In order to satisfy the conservation of mass and momentum, the final state (P_B, v_B) must also lie on the Rayleigh line as shown in Figure 3.

Simultaneously solving Equations 1 and 3 by eliminating D instead of u, the result would be an expression for u, the gaseous product velocity in the fixed reference frame.

$$u^2 = (P_B - P_A) (v_A - v_B) \tag{5}$$

Figure 4 shows several curves of constant u plotted on a P-v diagram. Solving Equations 1 and 2 for $u_B = (D-u)$ one would obtain
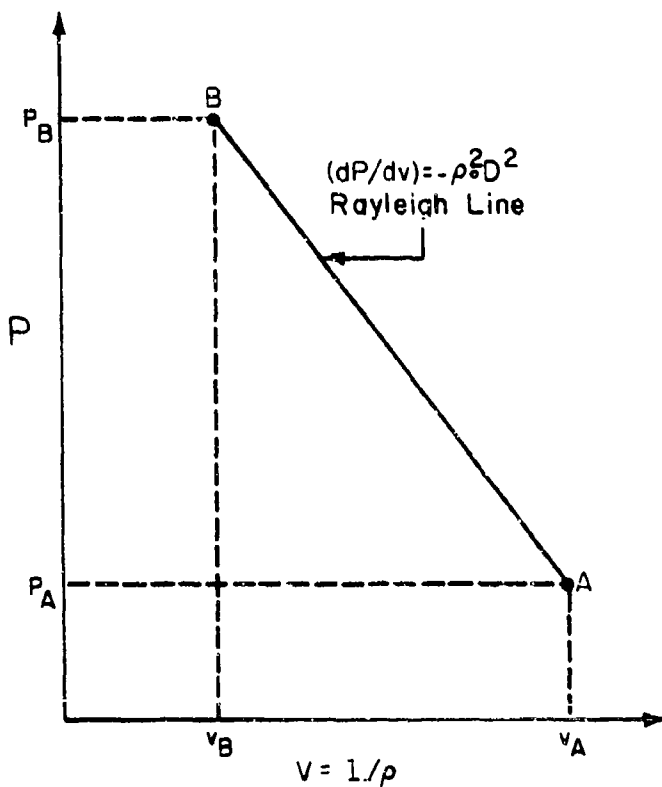
Fig. 3.   Illustration of Rayleigh Line.
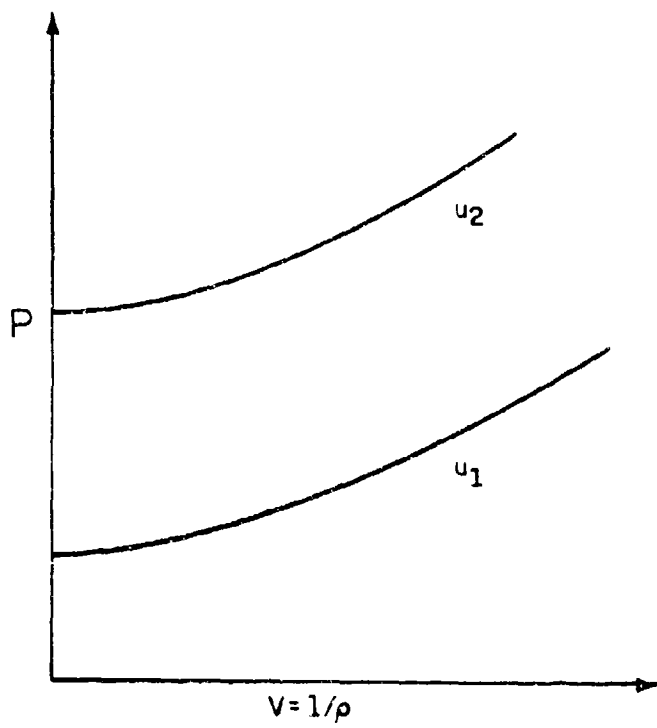
Fig. 4. Curves of Constant Product Velocity.

$$u_B^2 = v_B^2 (P_B - P_A)/(v_A - v_B) \tag{5a}$$

Equation 5a will be important later in showing that for a CJ detonation the product velocity is sonic with respect to the detonation front.

The third conservation equation, the conservation of energy across the reaction zone, can be written

$$E_{int_A} + P_A v_A + \frac{1}{2} D^2 = E_{int_B} + P_B v_B + \frac{1}{2} u_B^2 = E_{int_B}$$
$$+ P_B v_B + \frac{1}{2} (D-u)^2 \tag{6}$$

In Equation 6, E_{int} represents the specific internal energy at each respective location and v is the specific volume $v = 1/\rho$. Since C_v, the specific heat at a constant volume, is assumed constant throughout the process, the internal energy at location B is simply

$$E_{int_B} = C_v T_B \tag{7a}$$

Likewise, the internal energy at location A is similar with the inclusion of the chemical energy yet to be released.

$$E_{int_A} = C_v T_A + E_{CHEM} \tag{7b}$$

By convention a positive value of E_{CHEM} is endothermic and a negative value exothermic.

Elimination of u and D from the energy equation (Eq. 6) is obtained by substituting in the mass and momentum equations (Eqs. 1 and 3). The result is a relation between E_{int}, P, and v in both reactant and product states known as the Hugoniot equation. It is expressed as

$$E_{int_B} - E_{int_A} - \frac{1}{2} (P_B + P_A)(v_A - v_B) = 0 \tag{8}$$

If one assumes that C_v is a constant and the reaction products obey an ideal equation of state

$$Pv = RT \tag{9}$$

then the internal energy expressions (Eqs. 7a and 7b) take the form

$$E_{int_B} = \frac{C_v P_B v_B}{R} = \frac{P_B v_B}{(\gamma - 1)} \tag{10a}$$

and

$$E_{int_A} = \frac{C_v P_A v_A}{R} + E_{CHEM} = \frac{P_A v_A}{(\gamma - 1)} + E_{CHEM} \tag{10b}$$

where γ is the ideal gas limit of C_p/C_v. Substitution of Equations 10a and 10b into Equation 8 gives a new form of the Hugoniot equation.

$$\left[\frac{P_B}{P_A} + \frac{\gamma-1}{\gamma+1} \right] \left[\frac{v_B}{v_A} + \frac{\gamma-1}{\gamma+1} \right] - 1 + \left[\frac{\gamma-1}{\gamma+1} \right]^2 = \left[\frac{\gamma-1}{\gamma+1} \right] \frac{2E_{CHEM}}{P_A v_A} \tag{11}$$

On a P-v diagram Equation 11 plots as a hyperbola passing through (P_A, v_A) for the case where $E_{CHEM} = 0$ and displaced from this point for increasing values of E_{CHEM} (see Fig. 5). From the solution of the conservation equations, the Hugoniot relation states that flow coming in at pressure $P = P_A$ and specific volume $v = v_A$ with chemical energy $E_{CHEM} = E_{CHEM_1}$, must have a final state (P_B, v_B) which lies on the E_{CHEM_1} Hugoniot. As discussed earlier, the Rayleigh line connecting the initial state (P_A, v_A) with the final state (P_B, v_B) dictates a unique solution for the detonation velocity, D, for that process. Therefore, the steady s ate flow process between states A and B shown in Figure 2 can be uniquely modeled by the Rayleigh line and Hugoniot curve on Figure 6, knowing the initial state (P_A, v_A), the final state (P_B, v_B) and the chemical energy E_{CHEM} of the re ctant. There are certain areas on the P-v diagram where a final solution to the flow process is impossible. For instance. the pressure and specific
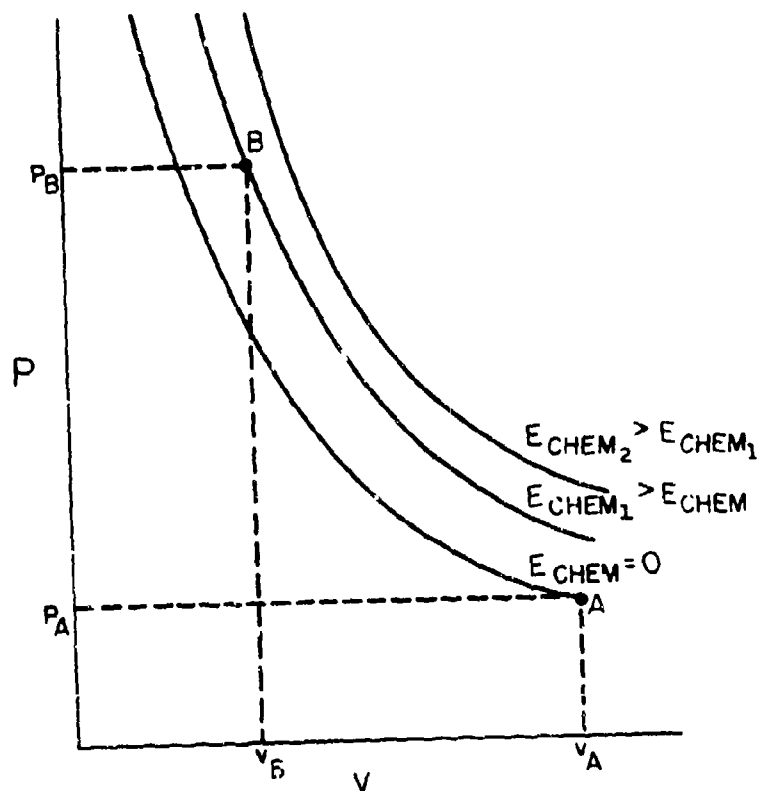
Fig. 5. Hugoniots for Three Different Values of Chemical Energy.

volume cannot both increase over the shock discontinuity.

Figure 6 shows a Hugoniot curve and two Rayleigh lines, R_1 and R_2, on the same P-v diagram. For Rayleigh line labeled R_2 there are two solutions labeled S for strong and W for weak. At the strong solution the flow downstream of the shock (u_B in Fig. 2) is subsonic with respect to the stationary shock, and a pressure disturbance initiated, traveling at the local speed of sound in the fluid, will propagate back and overtake the shock front. Looking at the same strong solution but in the fixed reference frame (moving detonation wave), a pressure fluctuation behind the detonation front (i.e., moving the rear wail in a closed system) will overtake the front and the front will adjust itself to that change. For the weak solution the flow behind the front (u_B in Fig. 2) moves away from the stationary front at a velocity greater than the local sound velocity. Therefore, a pressure disturbance in this case will not be felt by the front. Both the strong and weak detonations will be discussed in more detail in the next section.

In the case of the Rayleigh line labeled R_1 and the Hugoniot curve, there is only one unique solution to the conservation equations. At this point the two lines are tangent and the final st..te is identified as the CJ (Chapman-Jouguet) point. For this case, the flow behind the front at the CJ condition is moving at the local speed of sound with respect to the front (i.e., $u_B = a$).

In order to prove that the flow is sonic with respect to the detonation front, one should first look at the thermodynamic definition of sound speed.

$$a^2 \triangleq (\frac{\partial P}{\partial \rho})_s \equiv (\frac{\partial P}{\partial v})_s (\frac{\partial v}{\partial \rho})_s = (\frac{\partial P}{\partial v})_s (\frac{-1}{\rho^2}) \tag{12}$$
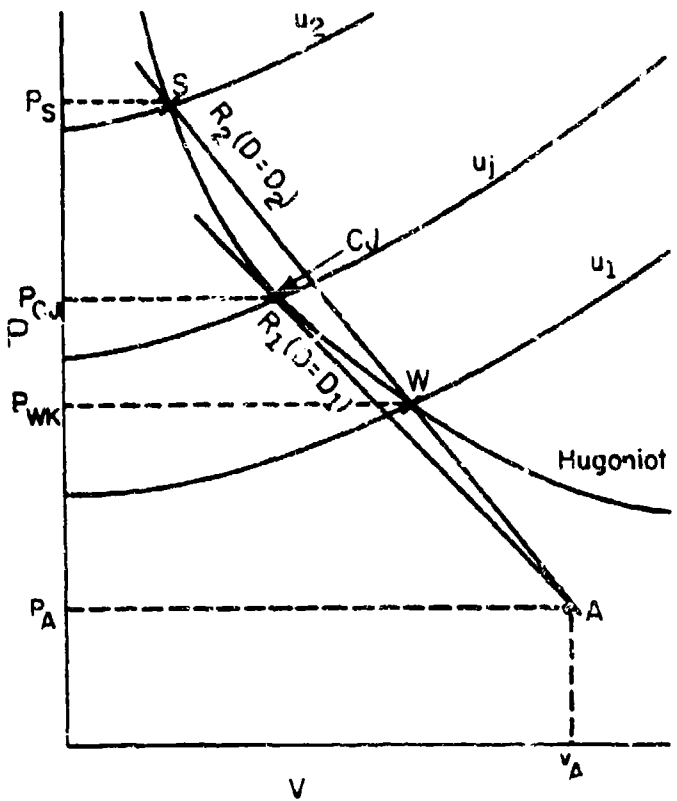
Fig. 6.   Pressure-Specific Volume Plot for One-Dimensional Flow
with Heat Addition. The Three Solutions Indicated (Strong,
Weak and CJ) are for the Case where $P_B > P_A$.

In Equation 12 the subscript s indicates the derivative is evaluated
at constant entropy. Therefore, for a detonation the local sound velocity
at the CJ point is simply obtained by evaluating the slope of an isen-
trope through that point on a P-v plot.

Since the slope of the Hugoniot and Rayleigh lines are equal at the
CJ point, it is useful to solve both derivatives and equate them. For
the Rayleigh line

$$\left(\frac{dP}{dv}\right)_R = -\rho_A^2 D^2 = -(P_B - P_A)/(v_A - v_B) \tag{13}$$

and for the Hugoniot curve

$$\left(\frac{dP}{dv}\right)_H = 2\left(\frac{dE}{dv}\right)_H / (v_A - v_B) + (P_B - P_A) / (v_A - v_B) \tag{14}$$

Equating the right hand sides of Eqs. 13 and 14 you obtain

$$\left(\frac{dE}{dv}\right)_{H_{CJ}} = -P \tag{15}$$

From the thermodynamic relation

$$dE = Tds - Pdv \tag{16}$$

you obtain

$$\left(\frac{\partial E}{\partial v}\right)_s = -P \tag{17}$$

by evaluating Equation 16 on an isentrope. Equations 15 and 17 imply
that at the CJ point an isentrope is tangent to both Rayleigh and Hugoniot
lines. From this

$$\left(\frac{\partial P}{\partial v}\right)_{s_{CJ}} = -\frac{(P_B - P_A)}{(v_A - v_B)} \tag{18}$$

Therefore, at the CJ point the local sound speed can be evaluated by using

Equations 12 and 18 to obtain

$$v_{CJ}^2 = v_B^2 \frac{(P_B - P_A)}{(v_A - v_B)} \qquad (19)$$

This is exactly the same as Equation 5a, the square of the product ve-
locity for a stationary detonation. Therefore, the product velocity for
a CJ detonation is sonic with respect to the detonation front.

From Equation 18, one can define gamma to be the negative logarith-
mic slope of the isentrope through the CJ point.

$$\gamma \equiv -(\partial \ln P / \partial \ln v)_s = \left[1 - \frac{P_A}{P_B} \right] \bigg/ \left[\frac{v_A}{v_B} - 1 \right] \qquad (20)$$

The analysis of detonation processes presented in this section as-
sumes γ is not only a constant value but is the same in both product and
reactant sides of the detonation wave. For most gases γ is about 1.2 [7].
In the case of a solid (explosive) detonating, Fickett and Davis [5] use
a value of $\gamma = 3.0$ and assumes the ideal state equation holds for the
product gases. From this assumption and estimate of γ, one could directly
apply the analysis formulated in this section to the solid detonation.

However, for two-phase reactive flow the mixture momentum and mix-
ture energy differ from Eqs. 3 and 4 by interactive stress and stress
work terms. Also, the gaseous products cannot be assumed ideal when ex-
perimental work shows detonation pressures of the order 15-20 GPa (2.17-2.9
Mpsi) [8]. Because of the high detonation pressure a nonideal equation
of state was implemented. This will be discussed in more detail in Chapter
2. Also, the jump conditions for a mixture with interactive terms is
outlined in Appendix A. It is similar to the material presented in this
section with the exception of the stress and stress work terms.

1.4 Rear Boundary Condition for Steady State Detonations

Reference 5 shows that the velocity, D, at which a detonation propagates into the reactants is dependent on the velocity at which the rear wall, or boundary, travels with respect to the CJ product velocity u_j. The product velocity was discussed in the previous section on the Rayleigh line and Figure 4 shows several curves of constant product velocity. The CJ product velocity would be the curve intersecting the CJ point in Figure 6. Three different possibilities for the movement of the rear wall with respect to the CJ product velocity exist and will be discussed in this section.

The first case to consider is where the rear wall velocity is greater than the product velocity at the CJ condition. On the P-v diagram (see Fig. 6) this would correspond to the solution labeled S for "strong". Here, the flow field following the detonation is constant with the product velocity $u = u_w$. Examining Figure 6, one can see that the final state pressure, P_B, is also greater than that of the corresponding CJ condition. Because the flow behind the detonation front is subsonic with respect to the front, any perturbation in the rear wall will propagate forward to the pressure front. Figure 7a shows a pressure profile for an overdriven detonation with the CJ pressure labeled on the figure.

The effects on the pressure by reducing the rear wall velocity can be seen in Figure 7b. Here, a rarefaction from the decreased wall pressure is shown propagating forward to the detonation front. An actual overdriven or strong detonation must have an external force driving the rear wall at a velocity greater than the CJ product velocity. Fickett and Davis [5] give as an example for an overdriven detonation the case where another detonation, stronger than the one being studied, is driving
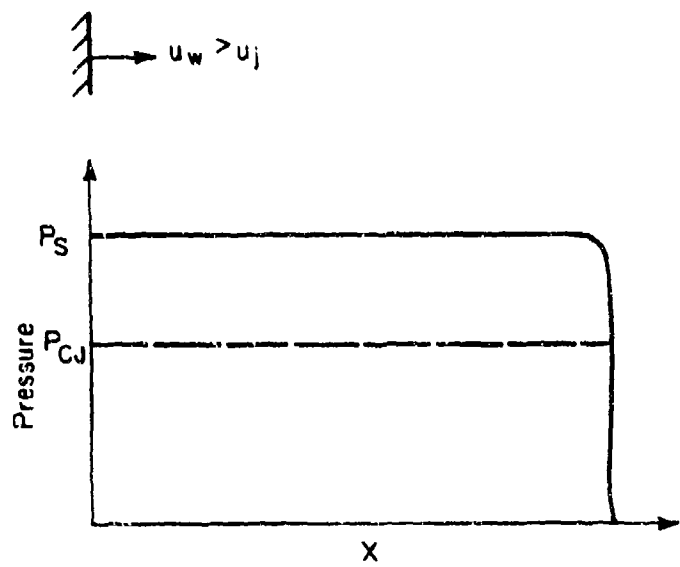
Fig. 7a. Pressure-Distance Plot for Case 1 ($u_w > u_j$).
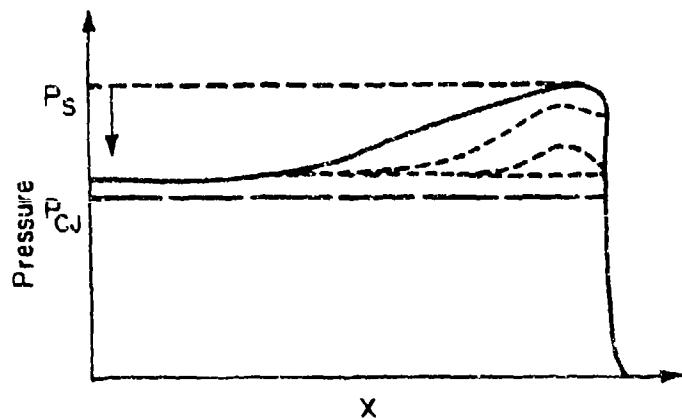
Fig. 7b. Case 1 with Wall Movement and Corresponding Pressure
Disturbance.

the rear wall.

A second possibility would be the case where the wall velocity is exactly equal to the product velocity at the CJ condition. Here, the detonation pressure is the CJ value and the flow following the front is sonic with respect to the front. Figure 8 illustrates case 2.

The third, and most important case for our study of DDT initiated by flame in a closed tube, is when the wall velocity is less than the CJ velocity. For this case, the front still propagates at the minimum detonation velocity allowable by the conservation equations, the CJ detonation velocity, D_{CJ}, and the combustion products leave at velocity u_j, sonic with respect to the front. Since the wall velocity is less than the product velocity, a rarefaction from the rear of the combustion zone to the wall is developed. This is an isentropic expansion characterized by the ratio of specific heat, γ, assumed for the products (see discussion in previous section). Figure 9 illustrates the case where the wall velocity is less than the product velocity. As an example of the isentropicity of the flow behind the front, the pressure ratio between the final reaction state (CJ) and the location labeled k in Figure 9 is obtained from the expansion wave

$$\frac{P_k}{P_{CJ}} = \left[1+(\frac{\gamma-1}{2}) M_k\right]^{2\gamma/(\gamma-1)} \tag{21}$$

where M_k is the Mach number of the flow at location k.

1.5 Steady and Unsteady Deflagration

Along with the three detonation solutions of the Rayleigh line and Hugoniot curves (i.e, CJ, strong solution, and weak solution) discussed in the previous section, there are other steady state solutions possible.
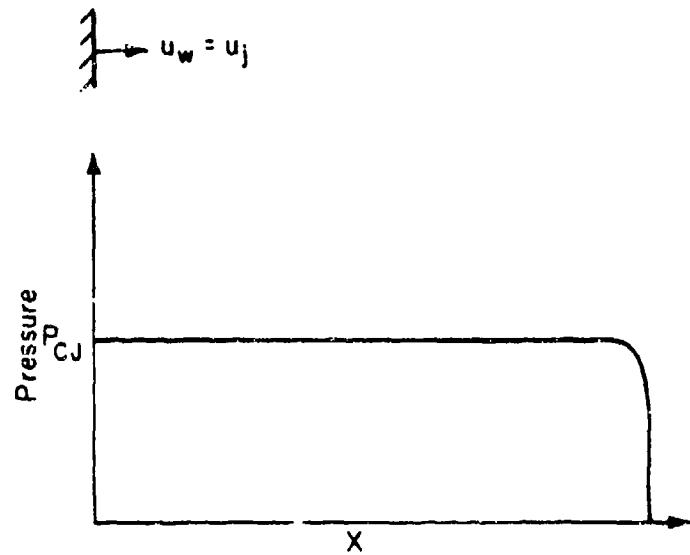
Fig. 8. Case 2 (Wall Velocity Equals Product Velocity).
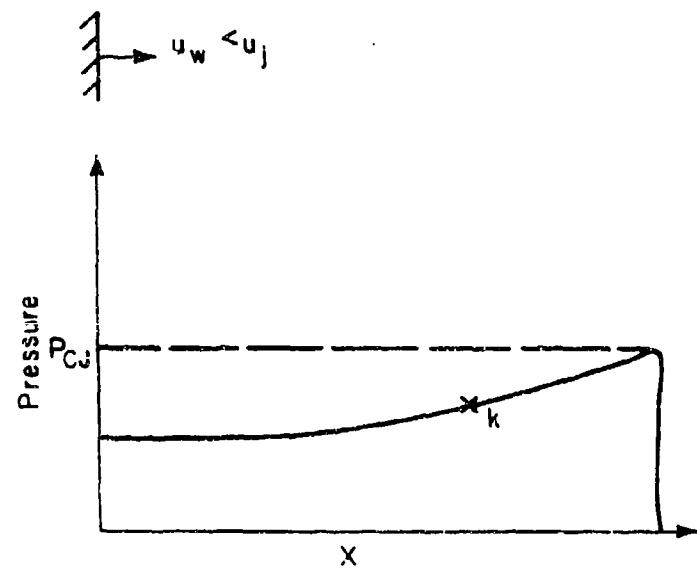
Fig. 9. Case 3 (Wall Velocity Less than Product Velocity).

Figure 10 illustrates a solution to the conservation equations on the lower,
or deflagration, branch of the Hugoniot curve. For this solution the
flame propagates through the unburnt reactants at a low Mach number (M<<1)
and as can be seen on the figure, the deflagration is characterized by a
drop in pressure and rise in specific volume across the reaction zone. Re-
call, for the detonation solution there was a rise in pressure and drop in
specific volume. An example of a steady state deflagration would be the
case of a flame burning on a bunsen burner. Here, the flame is stationary
and the reactant gas is flowing through the flame sheet at a low velocity.

When discussing DDT in a packed porous bed, one must clarify exactly
the fluid dynamics of the deflagration branch. At time t=0, one end of
the packed bed is ignited and generating gas from the propellant surface.
As time progresses, it is the hot gases confined in the region behind the
ignition front which in a sense drives the ignition front through the bed.

That is, unlike the pressure drop across the steady state deflagra-
tion solution, there is a pressure rise across the ignition front. The
increase in pressure is a result of the gas generation in the region be-
hind the ignition front being confined to a finite volume. Also, in the
analysis made of the steady state deflagration, all reaction was assumed
to take place across an infinitely thin reaction zone. I⁺ is obvious
that for the two-phase deflagration problem this is not the case. Be-
cause of the finite zone of reaction, the problem of the deflagration
flame is at most quasisteady and it may be that the nonsteady terms in
the conservation equations should not be neglected. Because of this
inherent unsteadiness of the deflagration phase of the DDT problem, the
reader should not confuse it with the steady state deflagration solution
shown in Figure 10. Later it will be shown that if transition from
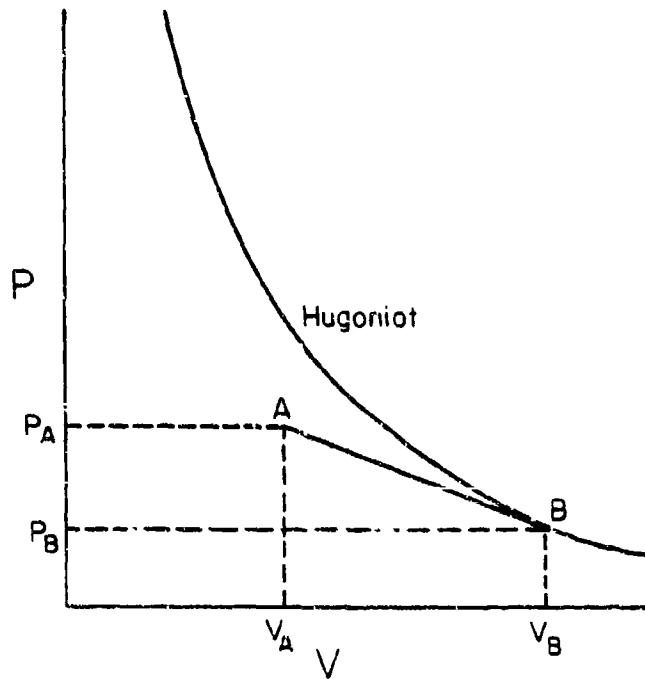
Fig. 10. Steady State Solution to Conservation Equations where $P_B < P_A$.

deflagration to detonation does occur, the reaction zone must collapse and a detonation solution can be analyzed as being steady and by the jump conditions being properly satisfied.

1.6 DDT in Two-Phase Reactive Flow (Experimental Data)

As discussed in the previous section, the transition from deflagration to detonation in a porous reactive medium is an unsteady process. Hot gases generated from the propellant surfaces are driven forward into the unburnt solid matrix by the pressure gradient developed at the ignition front. This phenomena is not found when a nonporous solid detonates, since only pressure disturbances can be propagated ahead of the ignition front. It is this convective heat transfer to the unignited propellant and the extended deflagration reaction zone which makes DDT in a porous bed unique when comparing it to DDT in either an all gas or an all solid regime.

Much experimental work on DDT in porous material has been carried out in the past decade. Bernecker and Price [8-10], have published the most recent results on DDT in a series of three papers. Other experimental studies prior to these include the work of Griffiths and Grocock [11] and Taylor [12].

The work presented in Reference 9 by Bernecker and Price is a study on DDT in RDX (cyclotrimethylenetrinitramine), a shock sensitive high energy explose. In their experiments the RDX was packed into a thick walled tube having an inside diameter of 16mm and being approximately 300mm (12 in.) in length (see Fig. 11a [8]). Both ends of the column were closed and ionization probes were located throughout the bed to trace the ignition front locus. The RDX was packed in an inert wax mixture and
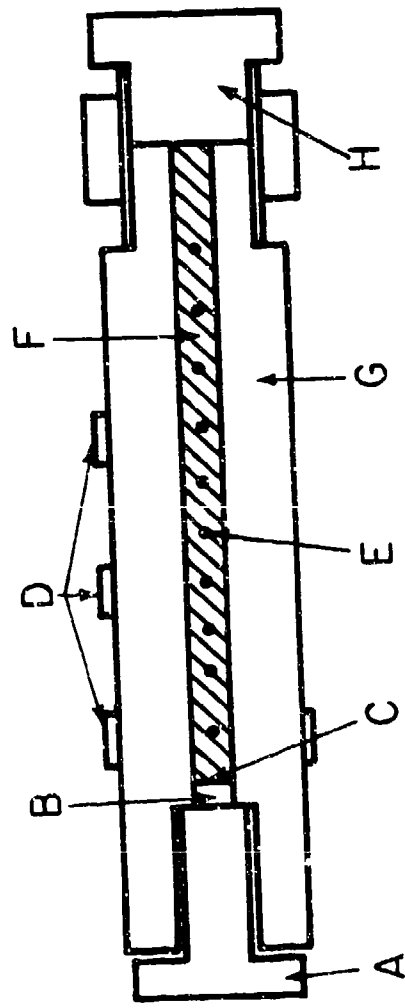
Fig. 11a. Schematic of Test Apparatus used by Bernecker and Price [8].
(A-ignitor bolt; B-ignitor; C-ignitor/explosive interface;
D-strain gages; E-ionization probe location; F-explosive
charge; G-tube; H-far end closure).

had a mean particle size of 200μm in diameter. Figure 11b illustrates the
DDT mechanism on a distance-time plot for the 91/9 RDX/wax granular charge
[9]. As shown in the figure, the convective flame front observed in their
work had no acceleration up to the detonation transition.

Their experimental work showed this convective ignition front traveled
at subsonic velocities (0.3-0.9mm/μsec) for most cases when the initial
porosities, ϕ_0, ranged between values of 0.1 to 0.3. The lower data points
on the plot represent a post convective compressional wave in the burning
region which overtakes the ignition front. The length of porous propel-
lant it takes for the compressional wave to overtake the ignition front
and transit into a detonation is ℓ_{CJ}, the run-up length.

1.7 Topics to be Addressed

The work presented in this chapter reviewed those features which dis-
tinguish DDT in a porous reactive medium from DDT in other media. Since
the work that follows in subsequent chapters will attempt to model this
phenomena, it was important that the properties of an actual detonation
be understood(Sections 3-5).

It was also pointed out that the DDT process being studied cannot re-
present the transition between the lower CJ point and the upper CJ point.
That is, because the flame propagates from a closed end and the deflagra-
tion reaction zone is never of infinitesim l thickness, one cannot apply
steady state jump conditions for the deflagration phase.

The chapter that follows reviews the past DDT modeling efforts and
inidcates how this work builds for the present effort. Numerical solu-
tions to the flow equations are carried out and solutions are presented
in Chapter 4. These results will show that the detonation (steady state
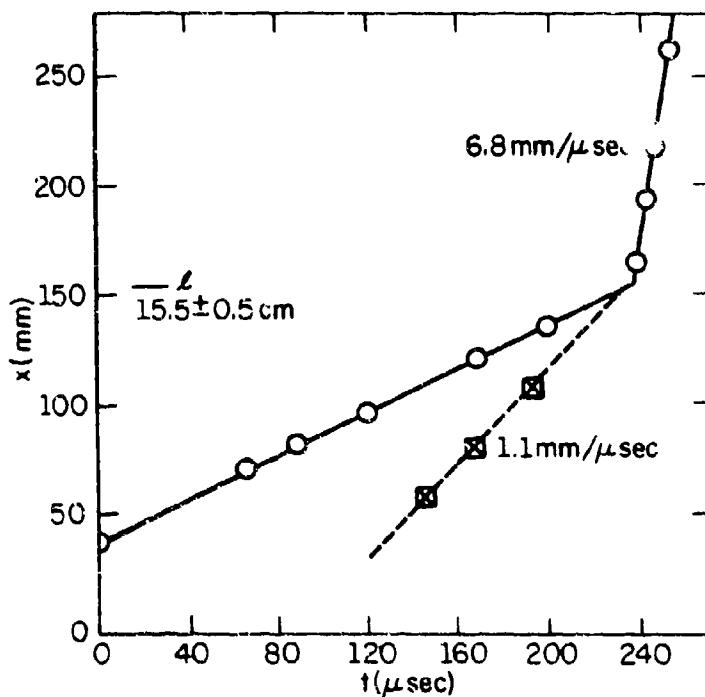
Fig. 11b.   Experimental Results for 78.8% TMD (ϕ_o = 0.22)
91/9 RDX/Wax; ρ_{o_p} = 1.32 g/cc. (Taken from Ref. 9).

supersonic wave) is a solution for a certain class of problems. Such results have yet to be presented by others.

CHAPTER TWO

THE MODEL AND ANALYSIS

2.1 Introduction

The analysis that follows attempts to model the situation in which a bed of tightly packed granular propellant is ignited at one end. Both ends of the packed bed are considered closed, thus, modeling the problem discussed in Section 1.4 where the velocity of the rear wall was less than the CJ product velocity. Recall for this case that after DDT, the detonation propagates through the unignited region at the CJ detonation velocity and detonation pressure and is followed by an isentropic expansion of the gases to the pressure at the stationary wall. The gas surrounding the particles at the initial time is considered inert, and to be at atmospheric pressure. It is also assumed that the inert gas will fully mix with the gases being generated from combustion of the propellant as time progresses. Figure 12 is a schematic of the propellant bed.

For numerical simplicity the propellant particles are assumed to be unsized spheres. Particles of interest range in diameter $50\mu m < d_p < 200\mu m$. To treat mult'-sized particles, one would require $\underline{N}$ independent equations of mass, momentum and energy for the solid phase, where $\underline{N}$ is the number of initially different-sized particles. A solids loading of 74% is the tightest possible for unsized spheres, obtainable by arranging the spheres in a face centered cubic. However, assuming granular deformation occurs under high stress loads, as discussed by Kuo [13], greater solids loadings may be predicted without error. Obviously, the spherical geometry must
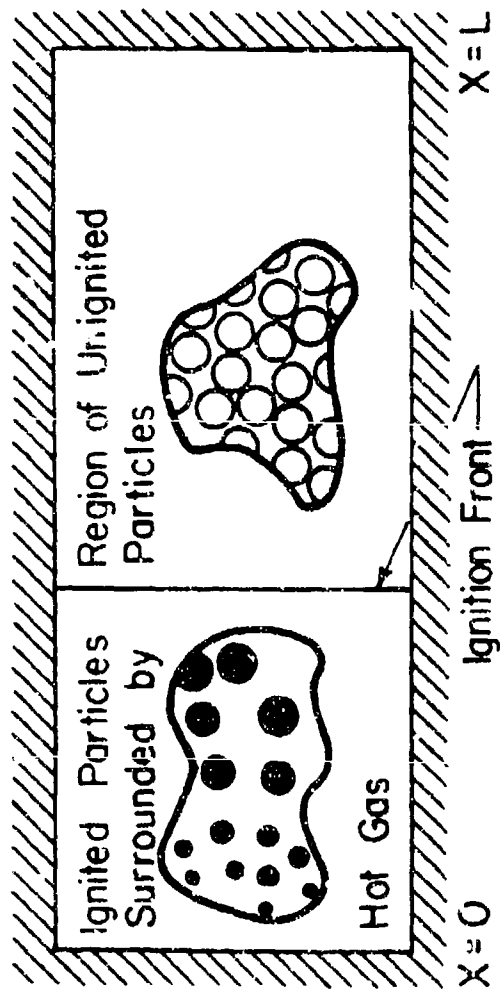
Fig. 12. Schematic of Packed Bed during Deflagration. Darkened Spheres Indicate Ignited Propellant Particles.

be altered for this to occur.

As the small fraction of propellant particles ignited at time t=0 burn, hot gases are generated as a function of the pressure-dependent burning rate law and surface-to-volume ratio $(3/r_p)$ of the spheres. These hot gases generated are convected forward through the lattice of unburned propellant and flow gradients develop, as dictated by the solution of the conservation equations and the necessary constitutive relations.

Heat transfer from the hot gases to the unignited propellant particles, dependent on the velocity of the gas relative to the particles and several gas properties (i.e. viscosity, thermal conductivity), transports energy from the gas to the solid phase. Subsequent ignition of particles further down the bed is assumed to occur when a _critical_ solid phase internal energy is reached [2]. This energy can be expressed as a critical increase in solid phase temperature, T_p, since the specific heat of the solid is assumed to be known.

As time progresses the gas pressure behind the ignition front increases due to the confinement of the gases from the closed rear boundary and the pressure-dependent rate of mass generation in the gas phase. Under certain conditions* the pressure gradient can develop into a shock front which overtakes the ignition front propagating through the bed. When this occurs the ignition front experiences the transition from deflagration to detonation discussed in Section 1.6.

At the transition point the ignited region (zone of gas generation) narrows in width and is followed by a region of all gas where the propellant

---

* These conditions will depend upon the solid chemical energy, granulation (size and loading), burning rate, ignition energy, etc.

particles are completely burned out (see Fig. 13). The thickness of the reaction zone is a function of the initial particle size and solids loading, and thicknesses approaching 1mm may be possible as $r_p \to 0$ and $\phi_o \to 0$.

2.2 Assumptions

In order to numerically model DDT in two-phase flow while retaining the physics of the problem, several key assumptions had to be made. These assumptions are similar to those made by previous investigators (Ref. 2 and 4).

(1) Both the solid and gas phases are independently treated as continuums requiring their own conservation relations.

(2) Each phase interacts with the other. This is modeled by the mass, momentum and energy interaction terms in the conservation equations.

(3) All propellant particles are unisized spheres.

(4) Ignition of a propellant particle is obtained when a critical energy, expressed as a particle temperature, is transferred to the solid.

(5) The propellant particles are initially surrounded by an inert gas at temperature, T_{g_o}.

(6) During combustion of the propellant, the gaseous products mix with the inert gas described in assumption (5).

(7) Both ends of the bed are closed allowing no gases to escape.

(8) The specific heats at constant volume, C_v, for both phases are constant.

(9) When the solid phase, at a given x-location in the bed, displays a porosity $\phi > 0.95$ and a particle volume one-tenth of its initial

3
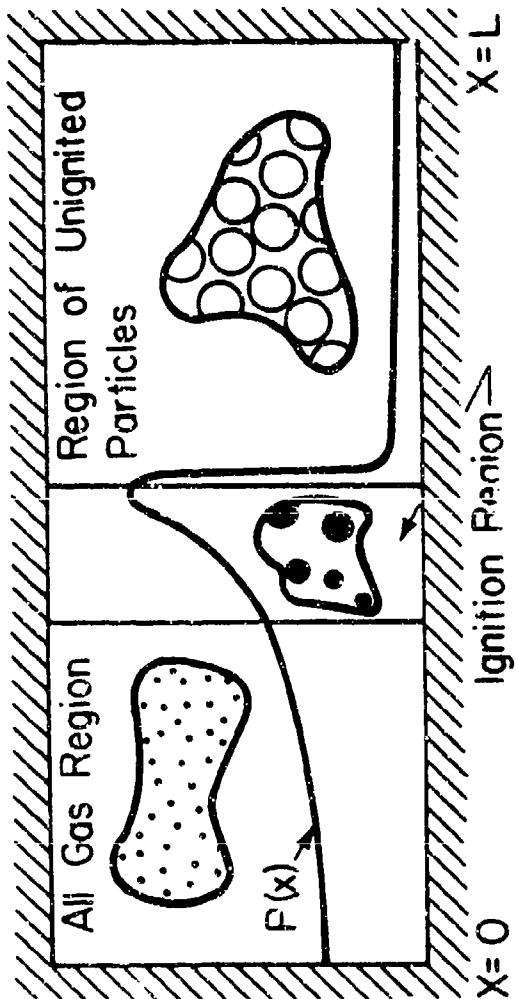
Fig. 13. Schematic of Packed Bed after Transition to Detonation. Ignition Region has Collapsed to a Thin Zone and is Followed by an all Gas Region.

volume, it is burned out and no longer generating gas. Results show this phenomena to proceed smoothly from the left boundary and thus not leaving any 'holes' in the continuum. This assumption was necessary to prevent a singularity from arising as $r_p \rightarrow 0$ and $\Gamma \rightarrow \infty$.

(10) All the product gases obey an assumed nonideal equation of state.

(11) The solid particles are compressible, without heating up, obeying a modified Tait equation of state.

(12) Once ignited, the particles are assumed to burn on the outer surface only, at a known pressure-dependent rate law.

(13) At some initial time, a "narrow" region at one end is ignited, burning at the low pressure prescribed.

2.3 Governing Equations

Numerical modeling of the two-phase reactive flow process in DDT involves the conservation of mass, momentum and energy per unit volume in both gas and solid phases. This is a system of six conservation conditions which form a set of nonlinear hyperbolic partial differential equations coupled by the interphase mass, momentum and heat transfer terms. The conservation equations for two-phase reactive flow have been developed previously and References 3 and 4 will provide the reader with the definitions, assumptions and expressions for the six following field-balanced conservation equations. The e are:

Gas Continuity

$$\frac{\partial \rho_1}{\partial t} = - \frac{\partial (\rho_1 u_g)}{\partial x} + \Gamma \tag{22}$$

Particle Continuity

$$\frac{\partial \rho_2}{\partial t} = - \frac{\partial (\rho_2 u_p)}{\partial x} - \Gamma \tag{23}$$

Gas Momentum

$$\frac{\partial (\rho_1 u_g)}{\partial t} = - \frac{\partial (\rho_1 u_g^2)}{\partial x} - \phi \frac{\partial P_g}{\partial x} - \mathcal{D} + \Gamma u_p \tag{24}$$

Particle Momentum

$$\frac{\partial (\rho_2 u_p)}{\partial t} = - \frac{\partial (\rho_2 u_p^2)}{\partial x} - (1-\phi) \frac{\partial P_p}{\partial x} + \mathcal{D} - \Gamma u_p \tag{25}$$

Gas Energy

$$\frac{\partial (\rho_1 E_{g_T})}{\partial t} = - \frac{\partial (\rho_1 u_g E_{g_T} + \phi u_g P_g)}{\partial x} + \Gamma \left[E_{CHEM}^g + \frac{u_p^2}{2} \right]$$

$$- \mathcal{D} u_p - \dot{Q} \tag{26}$$

Particle Energy

$$\frac{\partial (\rho_2 E_{p_T})}{\partial t} = - \frac{\partial (\rho_2 u_p E_{p_T} + (1-\phi) u_p P_p)}{\partial x} + \left[E_{CHEM}^p - \frac{u_p^2}{2} \right]$$

$$+ \mathcal{D} u_p + \dot{Q} \tag{27}$$

Here, the relations for the total internal energy in each phase are

$$E_{g_T} = C_{v_g} T_g + \frac{1}{2} u_g^2 \quad \text{and} \quad E_{p_T} = C_{v_p} T_p + \frac{1}{2} u_p^2$$

The subscripts g and p denote gas and particle respectively. In Equations 22 to 27, the phase densities, ρ_1 and ρ_2, are defined as

$$\rho_1 = \rho_g \phi \quad \text{and} \quad \rho_2 = (1-\phi)\rho_p$$

The porosity, ϕ, is defined as the ratio of the instantaneous gas volume to the mixture volume. Hence, the solids fraction is $(1-\phi)$.

In addition to the six conservation equations, three constitutive relations are needed in order to solve for the nine unknown variables; ρ_g, ρ_p, u_g, u_p, T_g, T_p, ϕ, P_g and P_p. These relations include state equations for both gas and solid states and a stress-resistance relation for P_p. Appendix B gives a complete listing of the relations used.

2.4 Improvements

Since the work reported in Reference 3, certain "improvements" in the modeling effort have allowed solutions which may be considered to be actual detonations. These improvements are discussed in some detail later in the text, but basically include:

1. Implementation of the necessary gas phase (nonideal) equation of state, to insure that at the CJ (Chapman-Jouget) conditions, the isentrope provides for a "gamma law" suitable at the hydrodynamic CJ state. (Appendix C presents a review of such an equation of state.)

2. Implementation of a new gas-particle friction coefficient, as developed by Wilcox and Krier [14], for flows at the high Reynolds numbers encountered in the developing DDT flows. Previously such coefficients were based on data only available for moderate Reynolds number ranges.

3. Utilization of a modified numerical integration scheme, which allowed for a reduction in the grid spacing (and hence reduction of the time increment) without the usual penalty of excessive computation costs and numerical instability that often follows when the total number of integrations is significantly increased.

2.5 Equations of State: Constraint Due to the Detonation State

As mentioned in Chapter 1, a nonideal equation of state must be utilized for the product gases. The analysis presented here uses a nonideal equation of state for hard spheres developed by S. J. Jacobs [15]. Previous to this study, a covolume-type state equation with data made available by Cook [16] was used (see discussion in Ref. 2).

The hard sphere equation of state takes the form

$$\frac{Pv}{RT} = 1.0 + b\rho + c\,(b\rho)^2 + \ldots \tag{28a}$$

where the constants b and c are determined by the value of the gamma law coefficient, γ, for the product gases as discussed in Appendix B. As stated, γ is the negative logarithmic slope of the isentrope tangent to both the Rayleigh and Hugoniot lines at the CJ point in the detonation state. That is, the slope of the isentrope that the product gases expand along in the product state. The reader may refer to Appendix C for the complete solution of the constants b and c.

Values for γ range from two to three for detonating high density explosives [15]. For the baseline case considered in this study, a value of $\gamma = 2.05$ was selected and the corresponding nonideal equation of state is:

$$\frac{Pv}{RT} = 1.0 + 2.5\,\rho_g - 0.50\,\rho_g^{\,2} \tag{28b}$$

When the above coefficients (2.5 and 0.50) were altered to treat a case for $\gamma = 3.0$, excessively high gas and particle temperatures were predicted as one might expect. In addition, during the numerical integration severe oscillations in gas and particle temperatures occurred in most cases when $\gamma > 3$. Since one is always constrained by the numerical integration schemes

that are employed to handle very severe gradients in the flow, it is under-
standable that previous efforts in DDT modeling [2, 3], which without
knowing were utilizing high γ values for the product gases, almost always
ran into numerical failure.

Evaluating the covolume state equation previously used in Ref. 3, an
approximate value of $\gamma = 3.6$ is calculated. This extreme value for γ may
be one important reason why the calculations, as reported in Ref. 2-4,
were unable to handle the high pressures associated with steady state
detonations.

In the solid phase the particles obey a modified Tait equation allow-
ing for compression of the granules. This is written as:

$$\rho_p = \rho_{p_0} \left[\frac{3P_p}{K_0} + 1 \right]^{1/3} \tag{29}$$

wnere K_0 is the bulk modulus. Reference 3 discusses the Tait equation in
more detail. A typical value is $K_0 = 1.38$ GPa $(2.0 \times 10^5$ psi).

2.6 CJ (Detonation) State

In the text by Fickett and Davis [5] equations are presented for es-
timating detonation velocity, D_{CJ}, and the detonation pressure, P_{CJ}, for
a steady state detonation. These are given for a single phase explosive:

$$P_{CJ} = 2(\gamma-1)\rho_{p_0} E_{CHEM} \tag{30}$$

and

$$D_{CJ}^2 = 2(\gamma^2-1) E_{CHEM} \tag{31}$$

Here, ρ_{p_0} is the initial solid material density and E_{CHEM} is the chemical
energy liberated by burning the solid. Since the problem being considered
is two-phase (solid-gas), Eqs. 30 and 31 must be modified to account for

this by converting ρ_{p_o}, the initial solid density, to ρ_{2_o}, the initial

solid _phase_ density $\rho_{2_o} = \rho_{p_o}(1-\phi_o)$. For an initial solid density $\rho_{p_o} = 1994$

kg/m^3, an initial porosity $\phi_o = 0.30$, a chemical energy $E_{CHEM} = 5.48$ MJ/kg,

and assuming $\gamma = 2.05$, Eqs. 30 and 31 give respectively:

$$P_{CJ} = 16.06 \text{ GPa}$$

and

$$D_{CJ} = 5.92 \frac{mm}{\mu sec}$$

These equations were developed from the jump equations for one-phase flow
where the equation of state for the product gases was assumed ideal. Be-
cause of this, these equations should only be used to get a good esti-
mate of the detonation pressure and velocity.

In addition to Equations 30 and 31 another method was presented by
Fickett and Davis [5] for estimates of detonation pressure and detona-
tion velocity. This is Kamlet's Short Method and was developed by Kamlet
and Jacobs [17]. In the CJ state they are:

$$P_{CJ} = K\rho_{o_p}^2 (NE_{CHEM})^{0.5} \cdot 1000 \tag{32}$$

and

$$D_{CJ} = A(1+B\rho_{o_p})(NE_{CHEM})^{0.25} \cdot 31.62 \tag{33}$$

where the constants A = 2.23 (m-kg-s^{-1}(mole MJ)$^{-1/2}$), B = 0.0013
(m^3/kg) and K = 0.762 (Nm^4 kg^{-1}(mole MJ)$^{-1/2}$). Again, ρ_{o_p} is the initial
solid density in kg/m^3 and N the reciprocal of the gaseous molecular
weight in mole/kg. Equations 32 and 33 give detonation pressure and ve-
locity for a detonating solid explosive going to all gas in the product
state. To modify Equations 32 and 33 for the two-phase problem, ρ_{o_p}, the
solid density, is again converted to the solid _phase_ density $\rho_2 = (1-\phi_o)\rho_{p_c}$.

It should be noted that Equation 33 expresses detonation velocity as a function of propellant density, while Equation 31 shows it to be independent of density. Like Equations 30 and 31, Equations 32 and 33 should only be taken as approximations.

Using the same input as above, Equations 32 and 33 give respectively

$$P_{CJ} = 16.52 \text{ GPa}$$

$$D_{CJ} = 7.83 \frac{\text{mm}}{\text{μsec}}$$

2.7 Gas Permeability

One of the key constitutive relations required in the analysis is the gas-particle (interphase) viscous force, which governs hot gas penetration into the unignited region of the granular material. As presented in Appendix A:

$$D = \frac{\mu_g}{4r_p^2} (u_g - u_p) f_{pg} \tag{34}$$

where f_{pg} is the drag coefficient. Until recently, the packed bed correlations by Ergun or Kuo and Nydegger (as reviewed in Ref. 14) were utilized for f_{pg}. Thus, the modeling efforts presented in Ref. 3 and 4 used the expression of Kuo and Nydegger [18]:

$$f_{pg} = \frac{(1-\phi)^2}{\phi^2} \{276 + 5 (\frac{Re}{1-\phi})^{.87}\} \tag{35}$$

Equation 35 was developed for 460 < Re < 14,600. Here, Re is the appropriate Reynolds number, defined as:

$$Re = [(\phi u_g)\rho_g \, 2r_p]/\mu_g \tag{36}$$

Based on experiments at both high gas velocities and high Reynolds numbers, Wilcox and Krier [14] developed the correlation:

$$f_{pg} = 5.06 \times 10^5 \; r_p \; Re/u_g^2 \tag{37}$$

where u_g is given in m/sec, r_p in meters, and the constants 5.06×10^5 must have units of m/s^2. This expression is not valid for either very low gas velocities, since Equation 37 would give $f_{pg} \to \infty$ as $u_g \to 0$, or for very high gas velocities*, since $f_{pg} \to 0$ as $u_g \to \infty$. The equation was found to be fairly accurate for $10^3 < Re < (2 \times 10^5)$ and 15 m/s$< u_g <$ 150 m/s. While a straight forward comparison is not easy, the difference between the value for f_{pg} as predicted by Equation 35 versus that by Equation 37 can be seen in the example. At $Re = 10^4$ and $\phi = 0.4$, Equation 35 gives $f_{pg} = 53,600$ and Equation 37 gives a value of $f_{pg} = 5448$. To utilize Equation 37 one must specify the average gas velocity, u_g, and the particle radius, r_p, that were used to obtain the Reynolds number. A kinematic viscosity $\mu_g/\rho_g = 1.8 \times 10^{-6} \; m^2/sec$, a particle radius $r_p = 1.0mm$, and an average gas velocity $u_g = 30.5$ m/sec were used to obtain a Reynolds number $Re \cong 10^4$. From this particular example, the Wilcox/Krier correlation (Eq. 37) allows about 10 times the permeability, i.e., 1/10 the viscous drag force as correlated by the Kuo/Nydegger relation.

Solutions to the flow process leading to DDT, discussed in the following chapter, clearly indicate that sufficient gas permeability is necessary to allow for a detonation transition.

---

*Data from Ref. 14 was limited to $u_g < 300$ m/sec.

CHAPTER THREE

NUMERICAL INTEGRATION

3.1 Finite Difference Mesh

To solve the Eulerian formulated system of conservation equations discussed in Chapter 2 with the constitutive relations listed in Appendix B, the length of the bed being integrated over is divided into I segments, each a constant Δx in width (i.e., $x_j = j\Delta x$; $j = 1, 2, 3....I$). The value required for Δx will be discussed later in the chapter.

At $t = 0$ values of the nine independent variables; ρ_g, ρ_p, u_g, u_p, T_g, T_p, P_g, P_p and ϕ are initialized at each jth x-location in the grid. Before incrementing the primary variables (i.e. mass, momentum and energy) to the future time, $t = t_o + \Delta t$, the auxiliary variables in the equations (e.g., drag, gas generation, heat transfer) must be computed at the present time, $t = t_o$. The nine equations are then solved at the incremental time, $t = t_o + \Delta t$, by a modified Lax-Wendroff finite differencing scheme. This method along with another tested are presented in Appendix D. The second method, developed by Rubin and Berstein [19], was implemented for several test cases and proved to give results similar to that of the Lax-Wendroff scheme. However, to keep all results consistent, the Lax-Wendroff scheme was chosen as the integrator.

The time increment, Δt, over which the equations are solved is calculated by the Courant, Fredrichs, Levy stability criteria [20], for hyperbolic equations,

$$\Delta t = \frac{\lambda \Delta x}{(c + |u|)}$$

(38)

In Equation 38, the term c is the mixture sound speed and $|u|$ is the maximum gas velocity in the bed. Also, λ is a stability constant, less than unity. For most cases $\lambda = 0.5$ was used. This smaller time increment was necessary in order to integrate the equations when large gradients developed in the flow.

3.2 Initial and Boundary Conditions

To initialize the problem, the bed is assumed to be quiesent, i.e., at a constant gas temperature and constant gas pressure throughout the length of the bed. The spherical propellant particles are typically fixed at a constant solids loadings, although a variable initial porosity can be treated. Then to initiate the flow, the propellant at the first few grid points is assumed ignited and generating gas. To be consistent with the flat initial pressure profile, all gas and particle velocities at time $t = 0$ are set equal to zero.

In the past an exponential pressure profile was constructed at the initial time in order to speed up the deflagration process. This was inaccurate, however, in that it was unsupported (i.e., no fluid motion was associated with the pressure gradient). Nevertheless, the computation time necessary for the pressure gradient to develop on its own was too great and the initial pressure gradient was implemented to speed up the process. Since then the computer code was modified to include an integration process which cuts the computation time drastically and allows for the use of a more realistic flat initial pressure profile ($P \simeq P_{atm}$).

Table 1 is a summary of typical input data for the cases studied.

3.3 Modification to the Integration Scheme

To solve on a digital computer the flow which is to represent a DDT

Table 1

TYPICAL INPUT DATA

PARAMETER	VALUE
Burning Rate Index	$0.8 < n < 1.2$
Burning Rate Proportionality Constant	$b = 0.001 \frac{in}{sec} \left[\frac{1}{PSI}\right]^{n}$
Initial Bed Porosity	$0.25 \leq \phi_o \leq 0.50$
Particle Diameter	$50 \mu m \leq d_p \leq 500 \mu m$
Bed Length	$L = 25.9$ cm
Grid Spacing	$\Delta x = 1.27$ mm
Chemical Energy	$4 \frac{MJ}{kg} < E_{CHEM} < 7 \frac{MJ}{kg}$
Gas Specific Heat	$1.0 \frac{KJ}{kg \cdot k} \leq C_{vg} \leq 1.9 \frac{KJ}{kg \cdot k}$
Initial Bed Temperature	$T_g = 294$ °K
Ignition Temperature (Bulk)	$T_{ign} = 303$ °K
Ignition Energy	$E_{ign} = 9.0 \frac{KJ}{kg}$

phenomena, requires the repetitive integrations of many equations. All of the conservation equations and constitutive relations are solved individually at each grid point in the entire bed, for each time increment.

A study of several test cases showed, for instance, that when the ignition front was at a given x-location, there was little activity several grid points ahead of it. That is, the gas and particles were at velocities close to zero and all transport coefficients were negligable in the region not far in front of the ignition front. This phenomena occurred for both the detonation state where the front was propagating between 5-8mm/μsec, and the deflagration state where the propagation velocity was much less. Because of this, an addition was made to the computer code which allows the code to only integrate the active region and bypass the inactive zone.

Ahead of the ignition zone, the computer code locates the nearest point to the zone where there is no significant particle or gas movement. This point is then designated as the new front boundary of the integration region for that particular integration step. When the pressure front builds the ignition front moves rather rapidly through the bed $(5-10\frac{mm}{\mu sec})$ and a new integration boundary must be located after each time increment.

Figures 14 and 15 show a comparison of a case run without the moving integration zone (Fig. 14) and one with (Fig. 15). To assure a correct solution the actual front integration boundary is extended a few grid points beyond the location calculated by the code. The addition of this new logic to the current code reduced computation time by at least one half, for the same time increment and grid space.

3.4 Artificial Smoothing

Inherent to the solution of the system of interdependent conservation
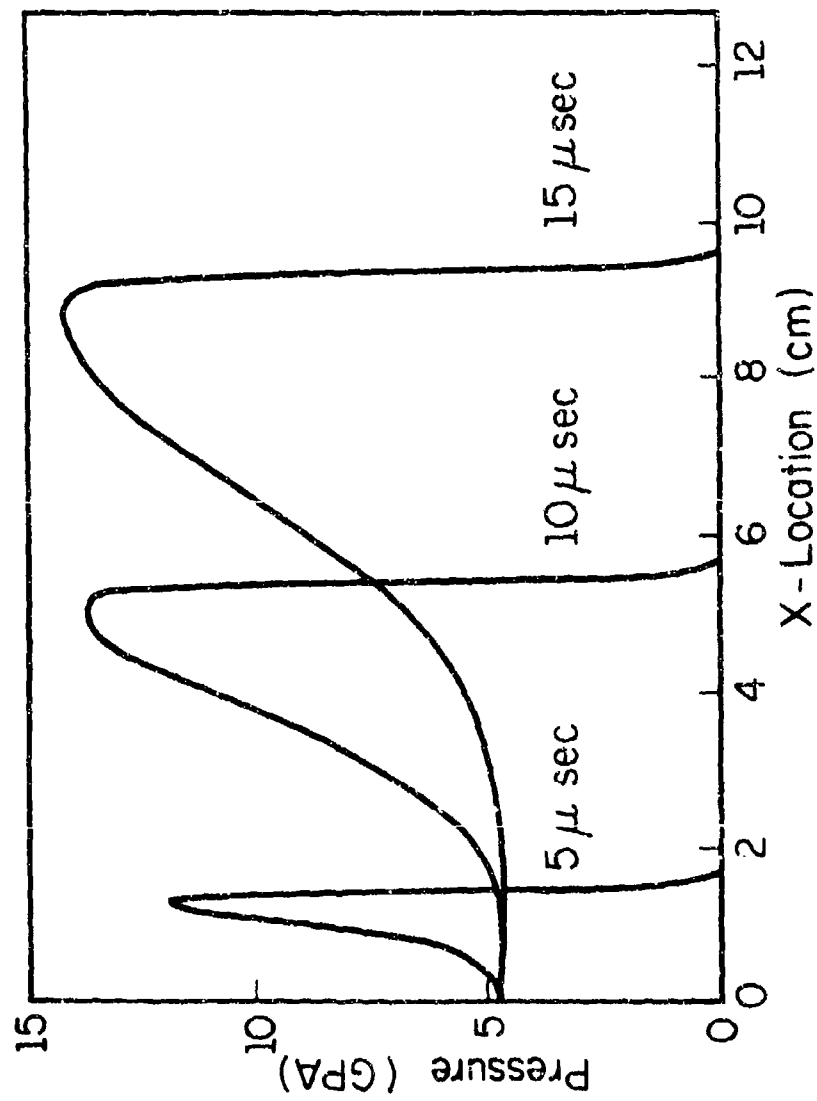
Fig. 24. Pressure-Distance Profiles for Case Run without Moving Integration Scheme.
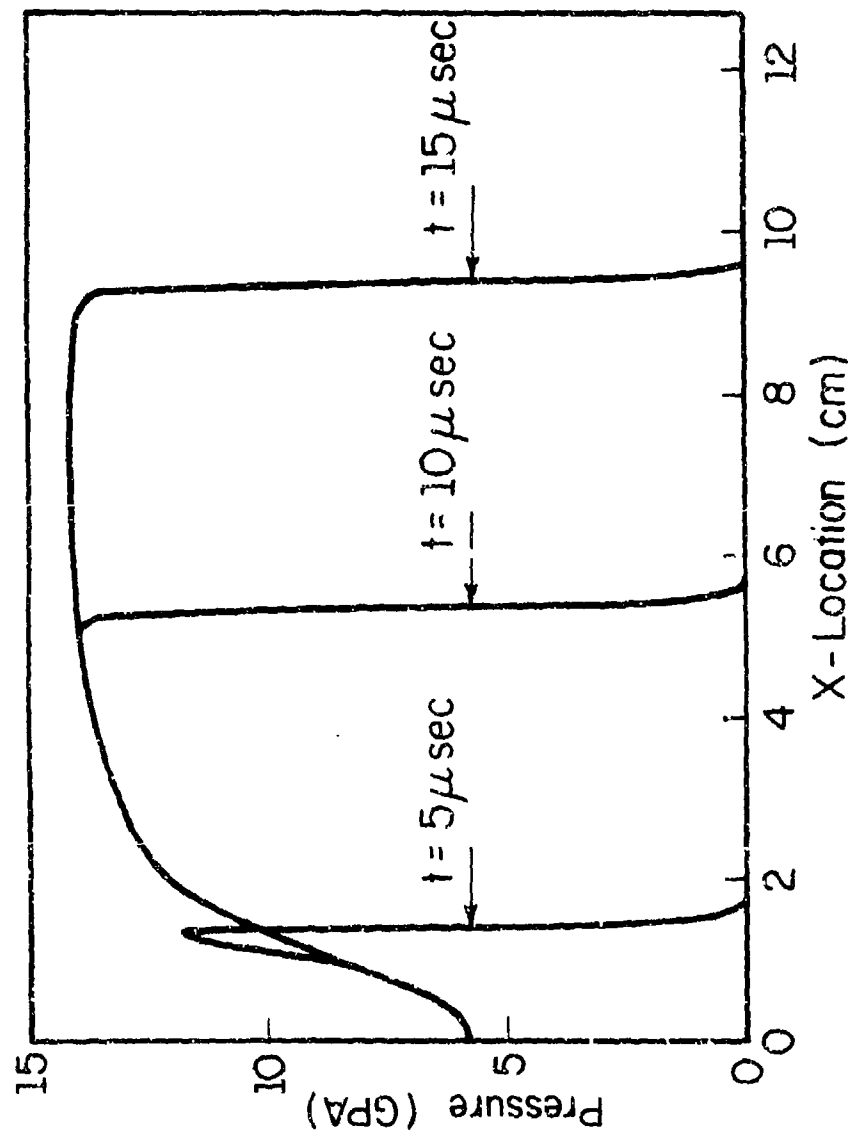
Fig. 25. Pressure-Distance Profiles for Case Run with Moving Integration Scheme.

equations is a numerical instability. A small perturbation can in some
cases amplify with each time increment and eventually destroy the numeri-
cal solution. This phenomena can start at the first time increment and
in ten to twenty integrations the oscillations can be so large that the
solution becomes unstable and terminates. In order to smooth out these
oscillations before they amplify, an artificial smoothing routine must
be incorporated into the code.

From experience in integrating the two-phase flow equations (Eqs.
22-27) with significant nonlinear source-sink terms, the problem of nu-
merical instability occurs often enough to warrant artifical smoothing.
An extensive study by the author and other investigators [2-4], shows the
final solution to be independent of any artificial smoothing used.

The analyzation of numerous test cases has shown, suprisingly, that
the stable solution did not require smoothing of all the variables. It
is obvious that the following results have an inherent dependency on
smoothing. Extreme care has been taken to minimize these effects on the
qualitative trends and quantitative results predicted. Nevertheless, it
should be obvious that smoothing techniques can supply variability in the
predicted parameters which are reflections of the scheme utilized, and not
necessarily of the conservation equations.

The particular artificial smoothing technique found to be useful is
a three point averaging technique where the variable ν determines what
weight is placed on each point. After the system of equations are solved
for at a given time, each variable in the vector U is recalculated by:

$$U_j^{new} = (1 - 2 \cdot \nu) U_j^{old} + \nu(U_{j-1}^{old} + U_{j+1}^{old}) \tag{39}$$

where

$$U = \begin{bmatrix} \rho_1 \\ \rho_2 \\ u_g \\ u_p \\ E_g \\ E_p \end{bmatrix}$$

For example, if $\nu = 0.1$ then U retains 80% of its original value and is influenced by 10% of the U values on each side. This is shown graphically in Figure 16.

For all cases studied, a minimum value of ν was used that would provide for a stable solution. This required repeating each test case numerous times, lowering ν each time until the solution went unstable.

3.5 Grid Spacing

It is obvious that in order to minimize computation time, a maximum value of Δx which gives a stable solution should be used. Based on the calculations carried out in References 2-4 a grid space of $\Delta x = 1.27$ mm was shown to be the largest Δx that would provide a solution to a flow problem which exhibited rather steep gradients.
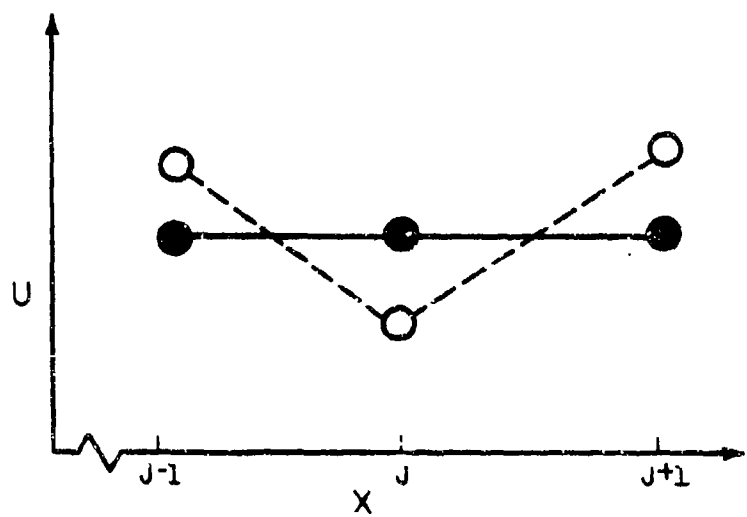
Fig. 16. Illustrations of Three-Point Artificial Smearing.
Open Circle Indicate Values of the Vector U Before
Smearing and Dots Denote the Values of U After Smearing.

CHAPTER FOUR

RESULTS COMPUTED

4.1 Introduction

This chapter will present the calculations made on the possibility of DDT occurring in packed beds of high energy, granulated, unisized propellants or explosives. It is obvious that there are an infinite number of loading combinations possible for the DDT study. Fortunately, the work of Hoffman and Krier [3] and Krier and Gokhale [2], in which conditions of rapid convective flame spreading have been calculated, is available and can be used as a starting point. It should be noted that none of the calculations made in References 2 or 3 predicted DDT. As pointed out in the previous chapters, there are probable reasons why this has not been accomplished and it is expected that certain improvements and modifications will now allow for the calculation of the steady state detonation solution.

The study made of a DDT potential attempts to model conditions similar to the test conditions of the Bernecker and Price work [9] (i.e., a long column of granulated material in a closed pipe ignited by an energetic ignition material at one end). In order to model the flow transient, one must assure that the length of the bed exceeds ℓ_{CJ}, the run-up length to detonation. Since the experimental work of Bernecker and Price [9] indicated that a 10 in (25 cm) bed was sufficient for most of their experiments where DDT occurred, this length was selected as the longest bed length to be considered.

Since unsized spheres are being treated, the initial porosity can be no less than $\phi_o = 0.26$, although randomly packed unsized spheres generally give a high porosity, about $\phi_o = 0.40$. Therefore, for this study $0.26 \leq \phi_o \leq 0.40$. The initial particle radii studied were also in the same range as those considered by References 2 and 3. Results in these studies showed that particles must be less than one millimeter in diameter in order to generate sufficient gases for the rapid flame spreading phenomena.

The chemical energy of the material considered is in the range of explosives or high energy propellants of the nitramine family (i.e., HMX, RDX). Thus, the chemical energies studied were always larger than 1000 cal/g (4.15 MJ/kg). Other parameters one must consider in the DDT studies are the burning rate properties of the propellant. Again, the values used in References 2 and 3, which attempted to model the burning rate of an HMX solid propellant, were utilized. However, the burning rate index, n, is a parameter which is explicitly studied.

In this analysis, the deflagration will be initiated by assuming at time, $t = 0$, that except for a small portion of the bed at one closed end, the bed is quiescent and unreacting. As has been mentioned in Chapter 3, a closed end situation is considered and hence at the two end points ($x = 0$, $x = L$) it is assumed that all flow gradients are zero and that the velocities of the particles and gas must also be zero.

The following section begins with a solution that indicates, for the first time, a steady state detonation can be predicted. This result is then compared to conditions where no such detonation solution occurs. Additional calculations will indicate the sensitivity of the initial porosity, ϕ_o, chemical energy, E_{CHEM}, burning rate index, n, and ignition

energy, E_{ign}, on the run-up length to detonation.

4.2 Calculations

Figures 17a and 17b present a case where a transition from deflagration to detonation has occurred. For this example, the burning rate index was n = 1.0, the chemical energy E_{CHEM} = 5.48 MJ/kg and the particle radius r_p = 127 μm (.005 in).

The pressure-distance profiles at five separate times after ignition of the propellant at x = 0 are shown in Figure 17a. Examining the profile for t = 50 μsec, one can observe that the profile is characterized by a shock front at x = 23 cm followed by a smooth expansion back to the wall at x = 0 cm. The pressure in front of the shock is at atmospheric conditions and, therefore, negligible with respect to the pressure behind the shock.

The ignition locus plot for this particular case is shown in Figure 17b. Here, the ignition front moves through the bed at a low subsonic velocity for the initial ten microseconds and then accelerates to reach a steady state velocity of D_{CJ} = 7.2 mm/μsec. This occurs within 12 to 15 cm from the ignited end. Note that these detonation solutions for P_{CJ} and D_{CJ} are in fair agreement with the approximations made in Chapter 2 (Eqs. 30 and 31) for the given input (E_{CHEM}, ρ_o, γ_j).

Obviously, hydrodynamic steady state analysis (like Eqs. 30 and 31) cannot guarantee that a transition from deflagration to detonation will occur. However, it seems that "critical" values of porosity (related to gas confinement), gas generation rates, and chemical energy will provide for a DDT. For example, when the burning rate index was lowered to n = 0.8, as shown in Figures 18a and 18b, the steep pressure front associated
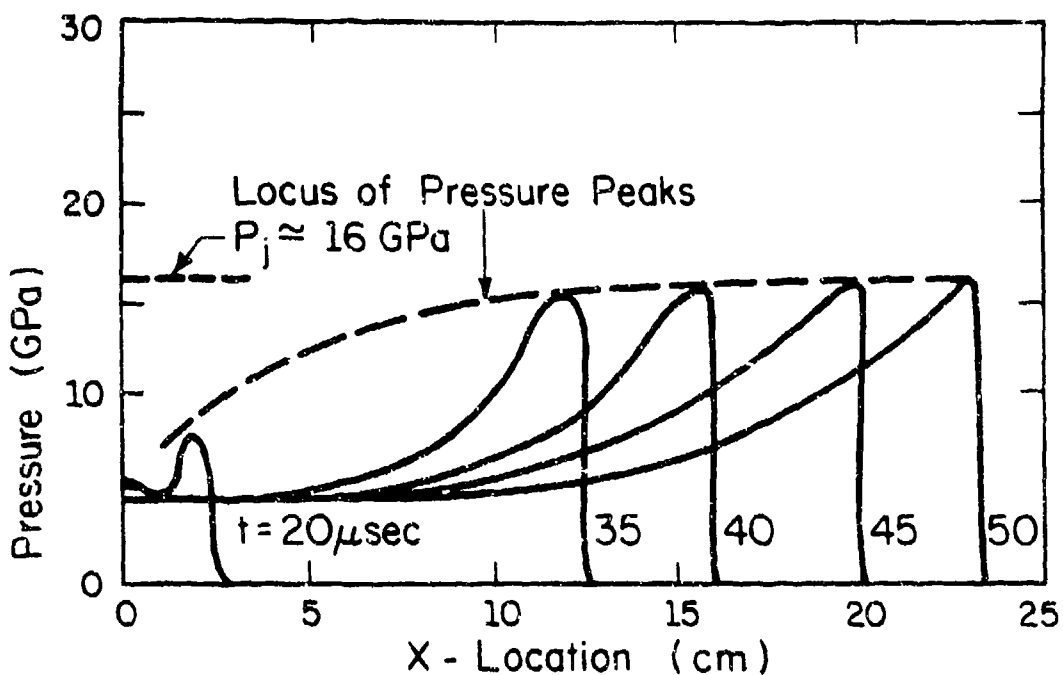
Fig. 17a. Pressure History During Accelerating Deflagration in a Packed Bed Leading to a Detonation Transition (n = 1.0).
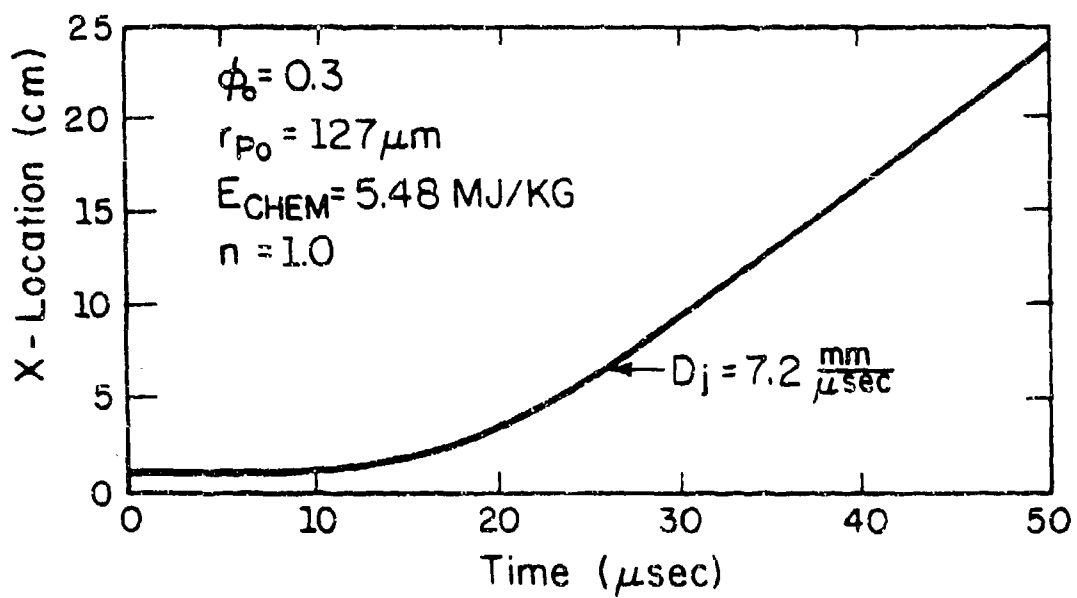
Fig. 17b. Ignition Front Locus with Detonation Transition (n = 1.0).

with a detonation did not develop. Correspondingly, no detonation speed
was predicted. In this example the peak pressure in the bed never ex-
ceeded 5 GPa, no shock was predicted, and only a steady convection-driven
front of 2.2 mm/μsec occurred at 100 μsec after ignition of $x = 0$. It is
not clear at this time whether or not this can be defined as a "low-ve-
locity" detonation.

According to Equation 30 in Chapter 2, for the case where a transi-
tion to detonation actually occurs, the steady state detonation pressure,
P_{CJ}, should increase linearly with the chemical energy, L_{CHEM}. Also, Equa-
tion 31 states that the detonation velocity, D_{CJ}, is a function of the
square-root of the chemical energy. Figures 19a and 19b present the re-
sults of a calculation where all parameters were identical to those used
to give the DDT results of Figures 17a and 17b, except $E_{CHEM} = 6.85$ MJ/kg,
an increase of 25%. The steady state shock pressure predicted for this
case, shown in Figure 19a, was 21 GPa. This represents a $(21/16.4 = 1.28)$
28% increase in pressure over the first case. The predicted detonation
speed (Fig. 19b), calculated from the slope of the x-t diagram, was 8.70
mm/μsec. According to Equation 31, the ratio of D_{CJ} for the case given in
Figure 19b to that presented in Figure 17b should be

$$\sqrt{(6.85/5.48)} = 1.12$$

This is approximately the increase predicted.

Table 2 summarizes the detonation pressure, P_{CJ}, and the detonation
velocity, D_{CJ}, (which were the end results of the DDT calculations) all
as a function of the propellant chemical energy. These predicted condi-
tions are compared with the approximate steady state hydrodynamic solu-
tions discussed earlier, i.e., Eqs. 30 and 31. The excellent agreement
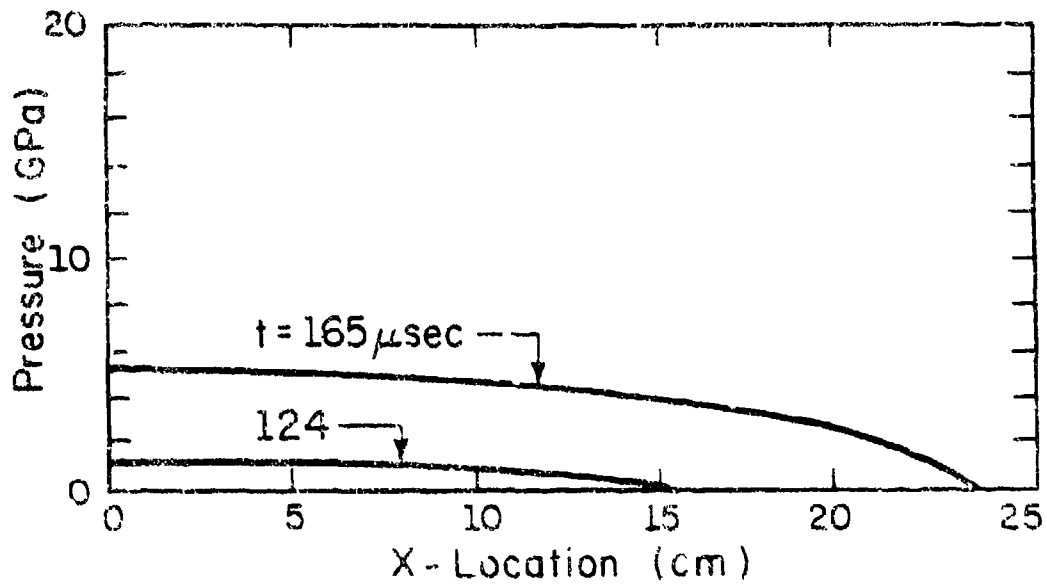
Fig. 18a.   Pressure History During Deflagration with no Transition
(n = 0.8).
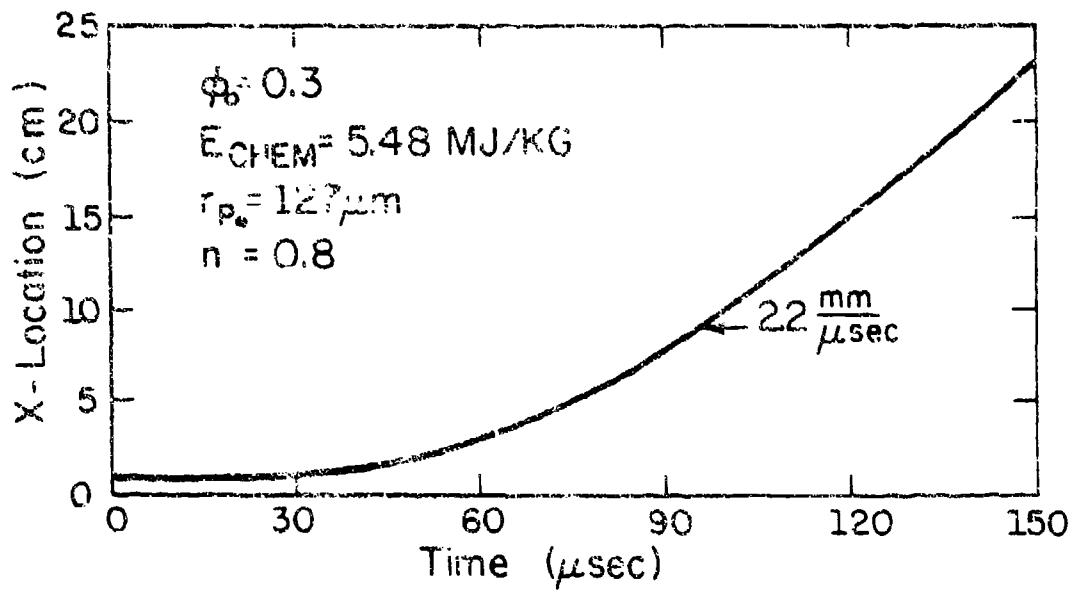

Fig. 18b.   Ignition Front Locus with no Detonation (n = 0.8).
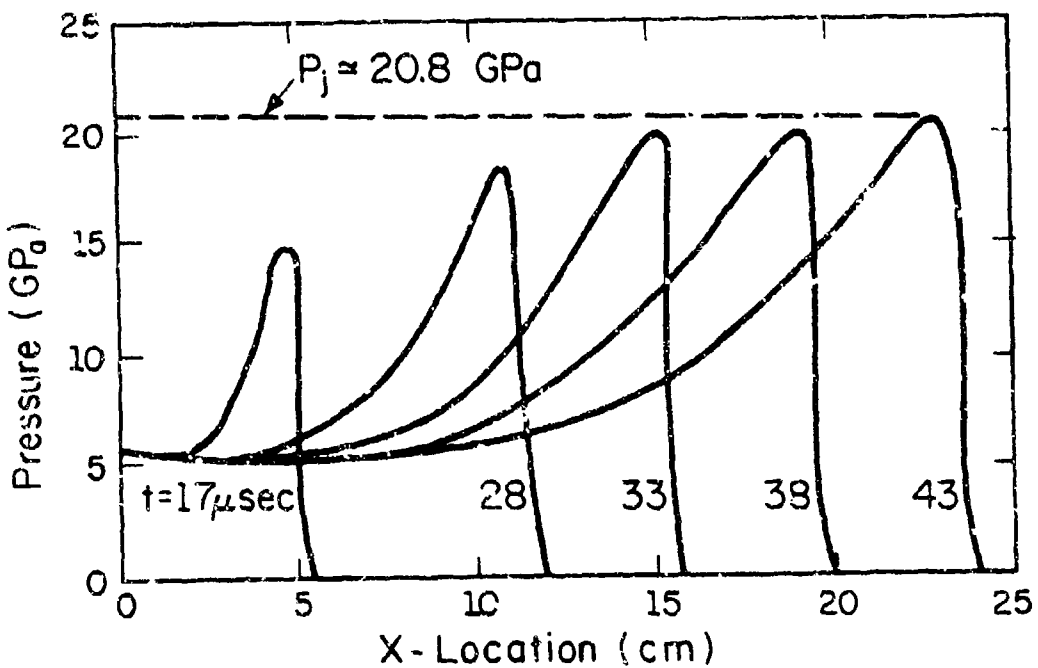
Fig. 19a. Pressure History Leading to Detonation with 25% Increase in E_{CHEM} (compare to case shown in Fig. 17a).
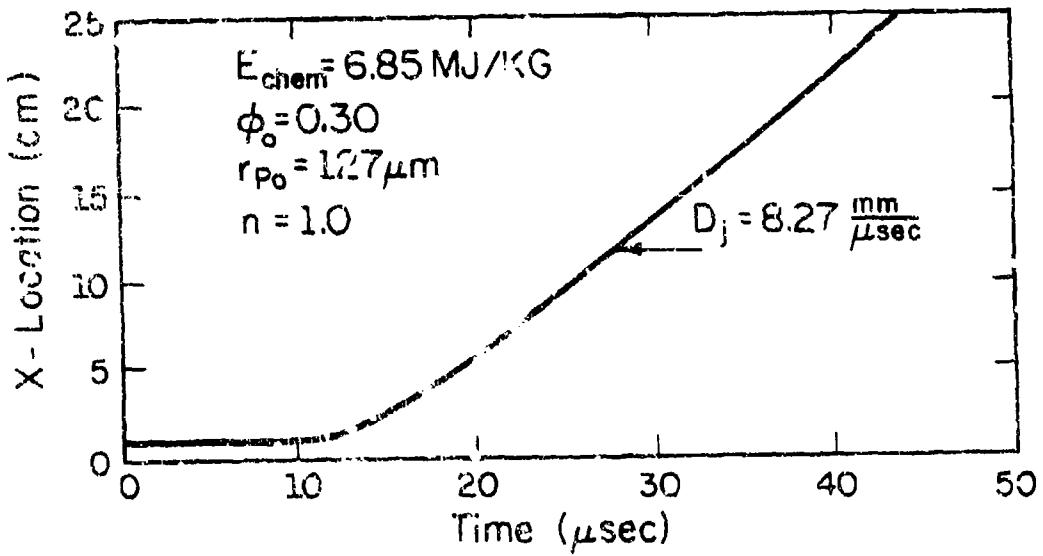

Fig. 19b. Ignition Front Locus (compare to Fig. 17b).

of the detonation pressure with the analytic solution should be noted.

However, the predicted value for the detonation velocity, D_{CJ}, from the hydrodynamic solution (Eq. 31) shows to be slightly less than the value predicted by the code for all cases. Although one cannot judge which of the two values, detonation velocity or detonation pressure, is more accurate, the percent increase in the detonation velocity as the chemical energy is increased compares favorably with the hydrodynamic solution.

4.3 DDT Run-Up Length

The run-up length to detonation is defined in this report to be the distance from the closed end where the bed is ignited to the location where both the peak pressure and the detonation speed are constant, i.e., the equilibrium steady state solution.

Figures 20a and 20b plot the predicted run-up length to detonation as a function of the burning rate pressure-index, n (Fig. 20a), and the initial bed porosity, ϕ_0 (Figure 20b). The "no-solution" boundary indicates that, with the integration scheme used, the mesh size would have to be drastically reduced (thereby decreasing the integration time increment) in order to obtain a stable solution. This is a costly exercise. but future work is planned to increase the solution regions. Figure 20a clearly indicates that, as expected, one cannot achieve detonation if the burning rate during the deflagration phase is not sufficiently large (see "no transition" boundary). For the solids loading considered $(1 - \phi_0 = 0.70)$, it would appear that a minimum DDT run up length is 5 cm for particles of 250 μm in diameter.

Figure 20b begins to resemble the required "U-shaped" curve of ℓ_{CJ}

TABLE 2

Comparison of the Predicted Detonation State with
an Approximate Hydrodynamic Solution

E_{CHEM}	P_{CJ} (predict 1)	P_{CJ} (Eq. 30)*	D_{CJ} (predicted)	D_{CJ} (Eq. 31)**	ℓ_{CJ}
4.11 MJ/kg	14.0 GPa	12.0 GPa	6.48 $\frac{mm}{\mu sec}$	5.12 $\frac{mm}{\mu sec}$	89 mm
5.48	16.6	16.07	7.25	5.92	51
6.85	21.8	20.08	8.24	6.62	44
8.22	24.6	24.1	9.17	7.25	38
10.96	30.0	33.2	10.58	8.37	28

$$* \ P_{CJ} = 2(\gamma_J - 1) \ \rho_p (1-\phi) \ E_{CHEM} \qquad \text{(Eq. 30)}$$

$$** \ D_{CJ}^2 = 2(\gamma_J - 1) \ E_{CHEM} \qquad \text{(Eq. 31)}$$
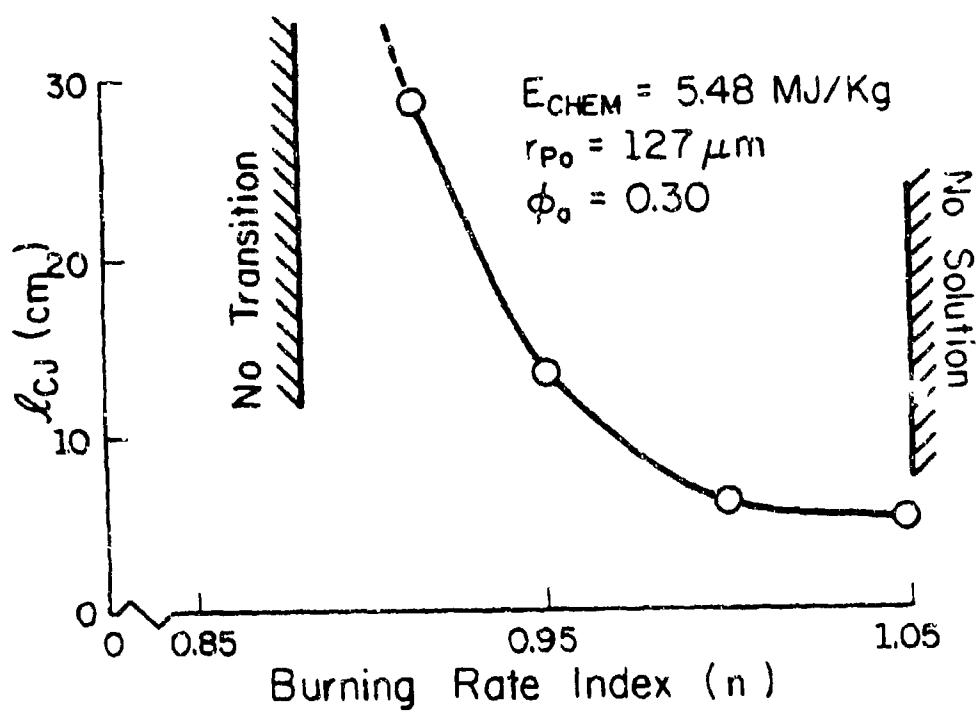
Fig. 20a.   Variation in Burning Rate Pressure Index, n, on Run-Up
Length, ℓ_{CJ}.

versus initial porosity. DDT experiments by Korotkov et. al. [21] show

a similar behavior (see Fig. 21). One would expect that for a relatively

porous bed, $\phi_o > 0.60$, no transition will occur since local pressure con-

finement is limited. If the porosity is too small no gas penetration

for the accelerating deflagration wave will occur. The net result is a

porosity where a minimum run-up length occurs.

Figure 22 presents a study on the effect of the chemical energy, E_{CHEM},

on the run-up length, ℓ_{CJ}, the values which were presented in Table 2.

As expected, the run-up length to detonation increases as the amount of

chemical energy decreases. Again, as expected there is a minimum value

where no transition occurs, $E_{CHEM} \doteq 3.0$ MJ/kg. For this case it does ap-

pear that a constant but small run-up distance is still required as the

chemical energy increases beyond the values studied here.

4.4 Detonation Reaction Zone

One measure of the fact that detonation occurs is a plot of the

reaction zone width versus the locus of the ignition front. This is pre-

sented in Figure 23, where the reaction zone is defined as the region

where particles are ignited and generating gas (i.e., are not burned out).

As shown, the zone initially increases during the deflagration phase as

the convective heat transfer provides energy to ignite more and more of

the bed. The zone then collapses to a thin (constant) width as the sur-

rounding high gas presssure causes the particles to burn out rapidly. A

steady reaction zone thickness of approximately 9 mm is predicted. How-

ever, most of the gas is generated in a small region immediately behind

the ignition front where the particles are still relatively large. Note

that in all the cases reported here, the initial particle diameter was
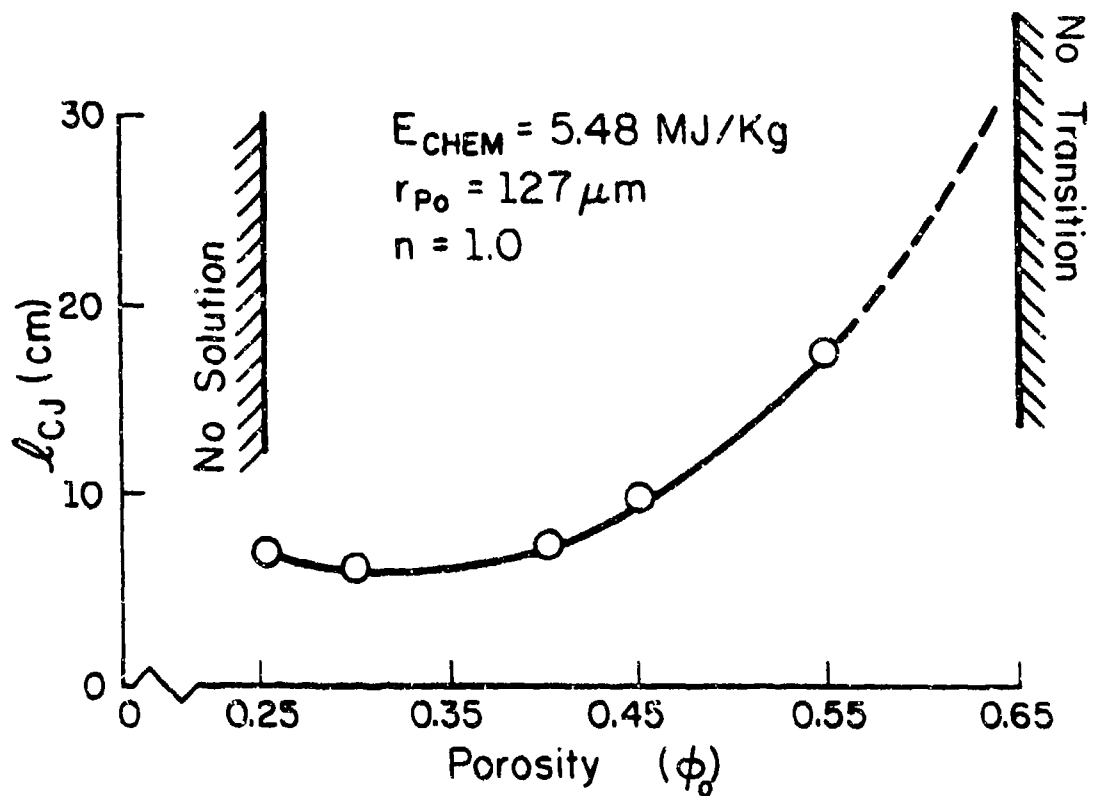
Fig. 20b. Variation in Initial Bed Porosity, ϕ_o, on Run-Up Length, ℓ_{CJ}.
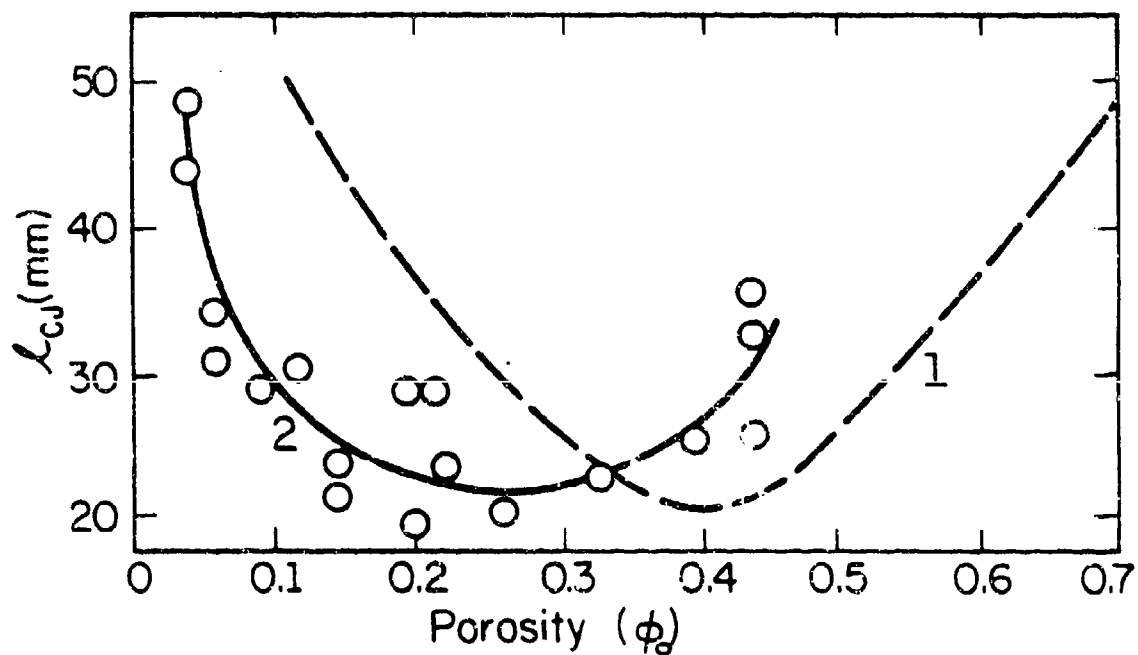
Fig. 21. Variation in Run-Up Length to Detonation with Porosity
for PETN (Ref. 21). 1. Fine (20 μm); 2. Coarse (500 μm).
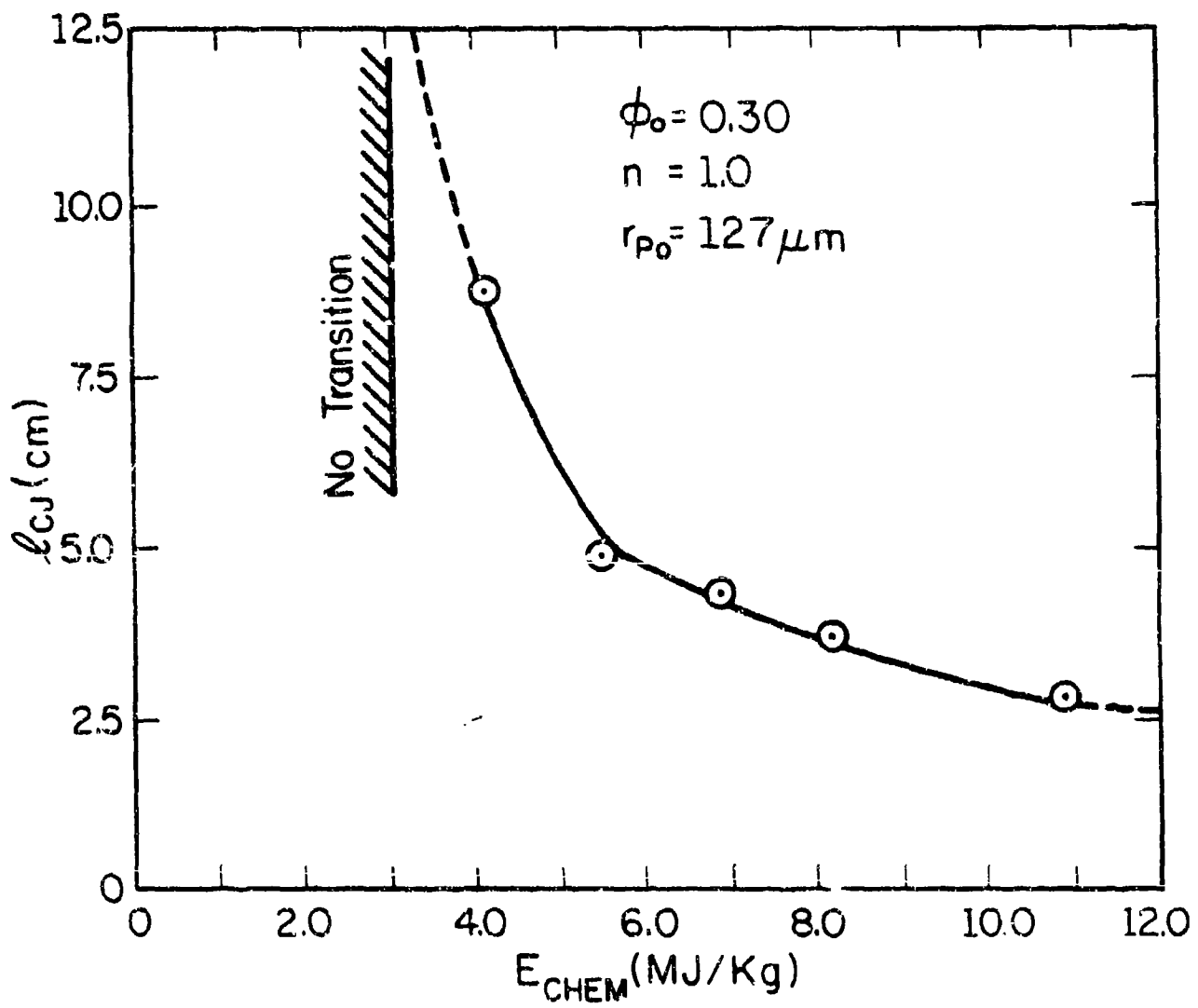
Fig. 22.   Variation in Run-Up Length to Detonation, ℓ_{CJ}, with Chemical Energy, E_{CHEM}.
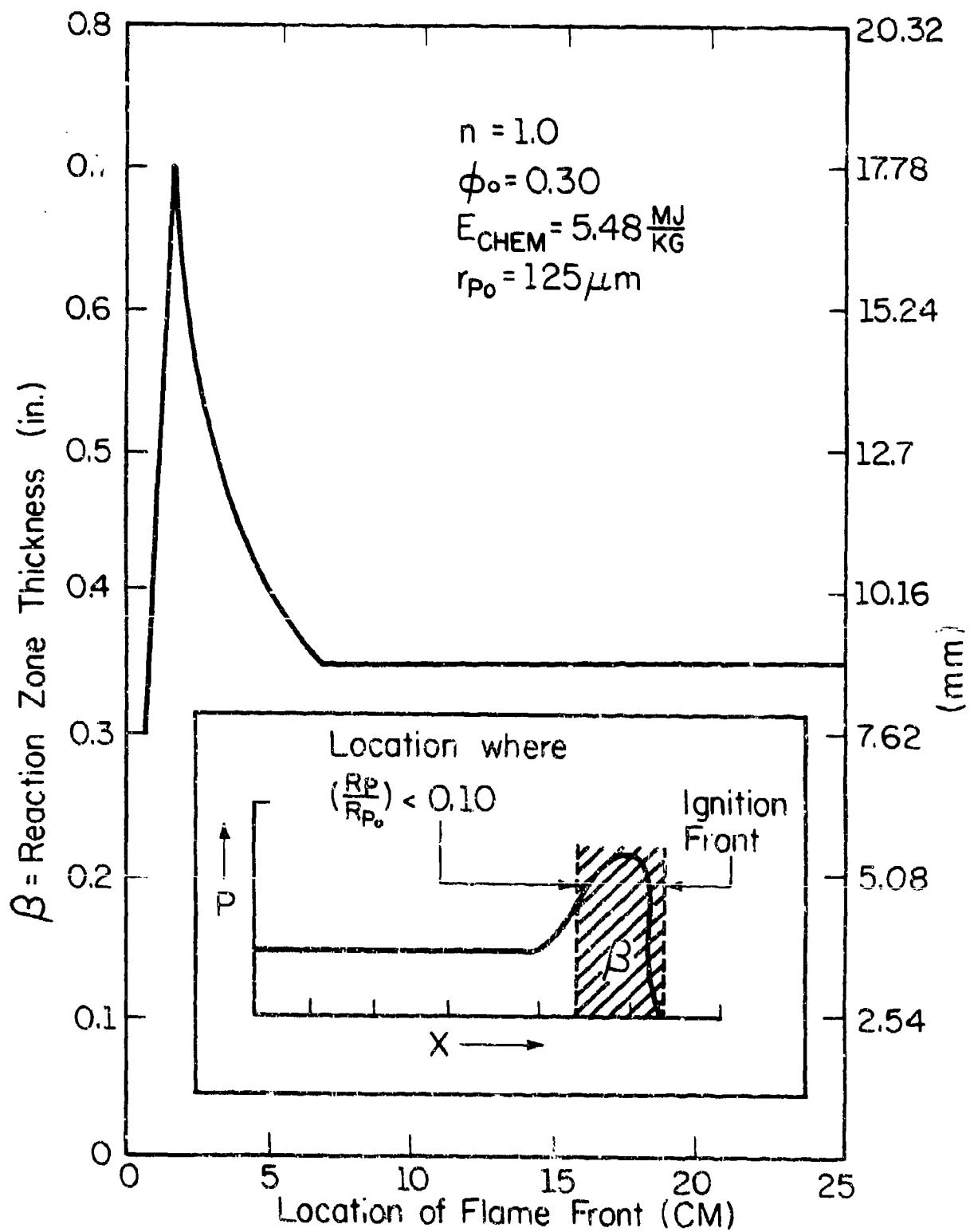
Fig. 23. Reaction (propellant gasification) Zone Thickness During an Accelerating Deflagration Leading to a Detonation.

250 μm. Obviously, smaller particles will provide for a thinner detonation reaction zone. Figure 24 presents a porosity-distance profile for a case where DDT occurred. Here, a porosity of ϕ = 0.95 is for all intents and purposes the condition when the propellant is burned out, i.e., no generation of hot gases.

4.5 Comments and Interpretations

The results shown in Figures 17-24 have clearly indicated that, as expected, high solids loading of relatively small particle size energetic propellant with perfect confinement will transit into a detonation in space domains of several centimeters. One would expect that propellant properties and packing configurations have limits where detonation cannot occur and this was clearly shown in some of the figures which show the run-up length versus property parameters. In conclusion, it will be useful to review these studies to determine the properties and configurations which minimize a DDT hazard.

For example, for a fixed chemical energy, E_{CHEM} = 5.48 MJ/kg, a fixed ignition energy, ΔE_{ign} = 9.0 KJ/kg, a fixed particle radius, r_{p_0} = 127 μm (0.005 in) and a fixed solids loading, $(1-\phi)$ = 0.7, the burning rate index, , must be larger than n = 0.86 if DDT is to occur. This was shown in Figure 20a. Of course, had the burning rate coefficient, b, been a different number, this exponent may have been different. A general statement can then be made that the burning rate, and hence rate of gas generation, should be kept as low as possible to minimize DDT. Conversely, the higher the burning rate, the better the chance of a transition to detonation occurring.

Figure 20b showed the run-up length to detonation versus initial porosity, ϕ_o. As was stated in the previous section, for all parameters
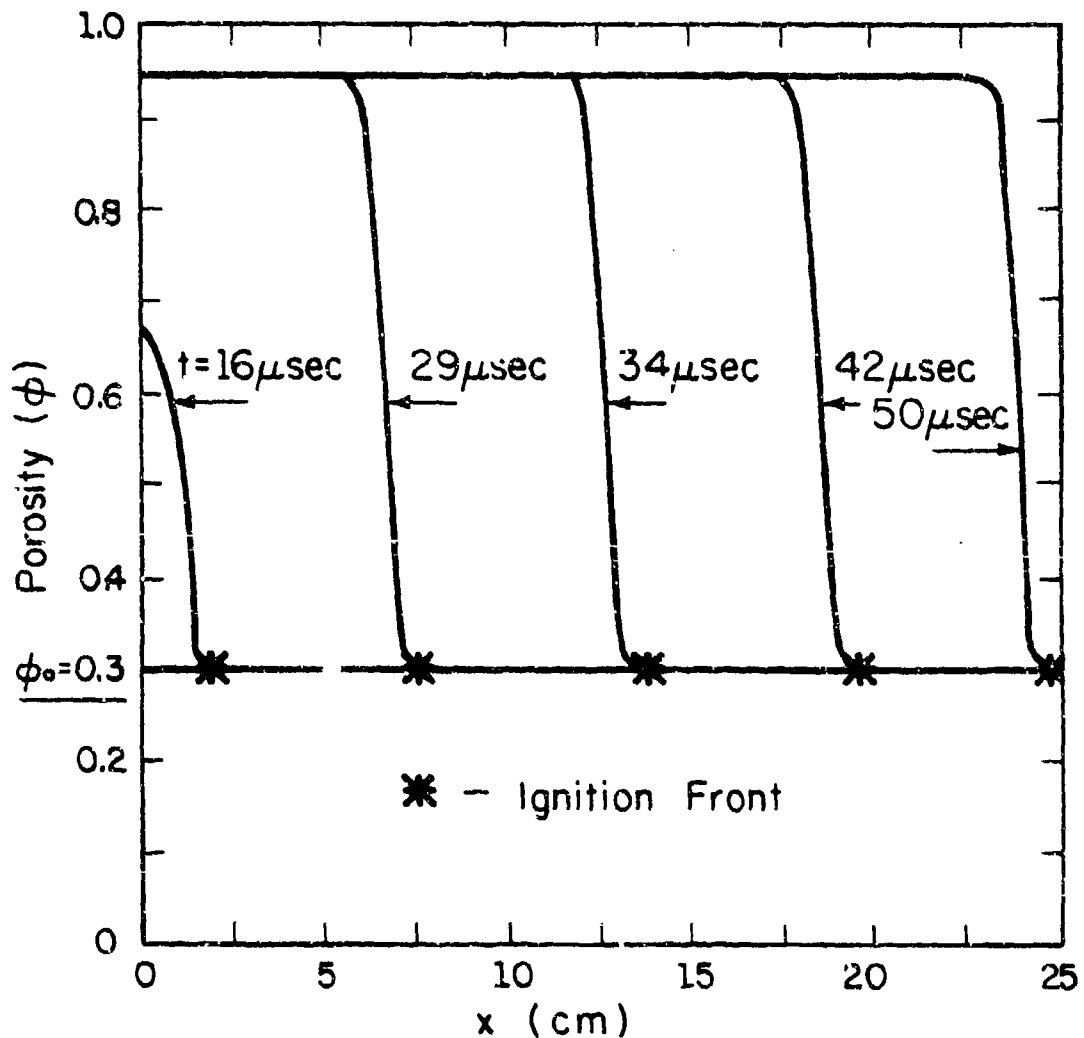
Fig. 24. Porosity-Distance Profile for a Case where DDT Occurred.

equal, there is a maximum initial porosity where no transition occurs.

Since a randomly packed bed of unisized particles has an initial porosity

of the order ϕ_o = 0.4, this figure indicates that this is in the region

where DDT potential is at a maximum. As one reduces the initial porosity

(that is increases the solids loading) the run-up length to detonation

slightly decreases until, as experimental work of Bernecker and Price [9]

has indicated, there is a mimimum initial porosity where DDT cannot occur.

Since at these initial solids loadings multi-sized particles and mechanical

packing are required, these loadings are not of interest, whereas the ran-

domly packed loadings are of interest.

A similar comparison of the run-up length to detonation was shown in

Fig. 22 where the chemical energy content was varied. Recall that a chemi-

cal energy, E_{CHEM} = 4.18 MJ/kg (1000 cal/g), can be considered an ener-

getic propellant material. Based on the results shown in Fig. 22, one

can state that less energetic material than this has little chance of en-

countering a DDT. Doubling the chemical energy from E_{CHEM} = 4.18 MJ/kg to

E_{CHEM} = 8.36 MJ/kg, represents a reduction in the run-up length of only

about one half. To summarize, high energy propellant of the nitramine

family where $E_{CHEM} \geq$ 4.18 MJ/kg, definitely fall within the regime of a

DDT hazard if properly confined.

The final comparison of this type is shown in Figure 25. This shows

the run-up length to detonation versus the particle radius. As one would

expect, there is a maximum particle radius (i.e., surface-to-volume ratio)

where transition is not predicted to occur. This is indicated by the "no-

transition" boundary on that figure. The figure also indicates that as

the particles get smaller in size, the run-up length to detonation also

decreases, as expected. Reducing the initial particle size, r_{p_o}, to
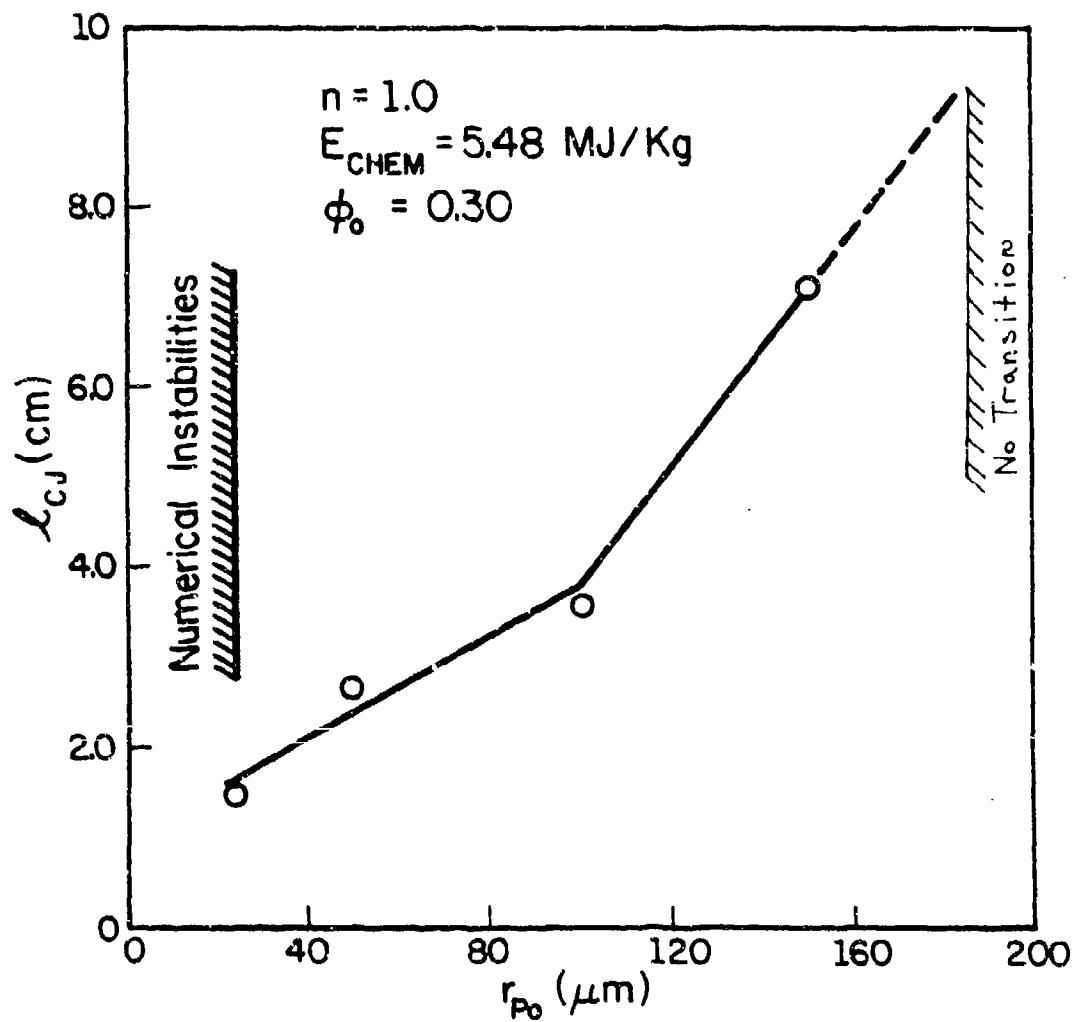
Fig. 25. Run-Up Length to Detonation Versus Initial Particle
Radius, r_{p_o}.

values less than 25 μm results in gas generation rates, per unit-volume, that are so large finer grid spacing must be utilized to assure stability. This expensive task has been delayed and is recommended only after improved numerical integration schemes have been developed.

A final topic studied dealt with the effect of ignition temperature (or more appropriately ΔE_{ign}) on the run-up length to detonation. For the results shown in this chapter a nominal value of $T_{ign} = 545°R$ was used. For this study $\phi_0 = 0.03$, $r_{Po} = 127$ μm and n = 1.0.

Calculations were made in which T_{ign} varied over the range $530°R <$ $T_{ign} \leq 575°R$. For a constant initial bed temperature of $T_{g_0} = T_{p_0} = 530°R$, this represents a range of ignition energy of $0.0 < \Delta E_{ign} \leq 25. \frac{kJ}{kg}$ For most of the ignition temperatures tested there was little change in the steady state detonation pressure or velocity. Only when ΔE_{ign} approached the improbable value of $\Delta E_{ign} = 0.0$ KJ/kg did the values change significantly.

REFERENCES

1. Van Tassel, W. F. and Krier, H., "Combustion and Flame Spreading Phenomena in Gas-Permeable Explosive Materials," International Journal of Heat and Mass Transfer 18, 1377-1386 (1975).

2. Krier, H. and Gokhale, S. S., "Modeling of Convective Mode Combustion through Granulated Propellant to Predict Detonation Transition," AIAA Journal 16 (2), 177 (1978).

3. Hoffman, S. J. and Krier, H., "Fluid Mechanical Processes of Deflagration to Detonation Transition in Beds of Porous Reactive Solids," Technical Report AAE 80-2, UILU-ENG 80-502, Aeronautical and Astronautical Engineering Department, University of Illinois at Urbana-Champaign, IL 1980.

4. Krier, H. and Kezerle, J. A., "A Separated Two-Phase Flow Analysis to Study Deflagration-to-Detonation Transition (DDT) in Granulated Propellant," Seventeenth Symposium (International) on Combustion, The Combustion Institute, Pittsburgh, PA, 1979.

5. Fickett, W. and Davis, W. C., Detonation, University of California Press, Berkeley, Los Angeles, London, 1979.

6. Strehlow, R. A., Fundamentals of Combustion, Robert E. Kreiger Publishing Company, New York, 1979.

7. Van Wylen, G. J. and Sonntag, R. E., Fundamentals of Classical Thermodynamics, John Wiley and Sons, Inc., New York, 1976.

8. Bernecker, R. R. and Price, D., "Studies in the Transition from Deflagration to Detonation in Granular Explosives - I Experimental Arrangement and Behavior of Explosives which Fail to Exhibit Detonation," Combustion and Flame 22, 111 (1974).

9. Bernecker, R. R. and Price, D., "Studies in the Transition from Deflagration to Detonation in Granular Explosives - II Transitional Characteristics and Mechanisms Observed in 91/9 RDX/Wax," Combustion and Flame 22, 119 (1974).

10. Bernecker, R. R. and Price, D., "Studies in the Transition from Deflagration to Detonation in Granular Explosives - III Proposed Mechanisms for Transition and Comparison with Other Proposals in the Literature," Combustion and Flame, 22, 161 (1974).

11. Griffiths, N. and Groocock, J. M., "The Burning to Detonation of Solid Explosives," Journal of Chemical Society, p. 4154 (1960).

12. Taylor, J. W., Trans. Faraday Soc. 58, 561 (1962)

13. Kuo, K. K., Moore, B. B. and Yang, V., "Intragranular Stress, Particle-Wall Friction and Speed of Sound in Granular Propellant Beds," Journal of Ballistics, 4, (1) (1980).

14. Wilcox, S. F. and Krier, H., Technical Report UILU-ENG 80-0501, University of Illinois at Urbana-Champaign (March 1980).

15. Jacobs, S. J., private communication with H. Krier and S. S. Gokhale, White Oak Laboratory, Silver Springs, MD, March 1978.

16. Cook, M. A., "An Equation of State for Gases at Extremely High Pressures and Temperatures from the Hydrodynamic Theory of Detonations," The Journal of Chemical Physics 15 (7) (1947).

17. Kamlet, M. J. and Jacobs, S. J., "Chemistry of Detonations - I - A Simple Method for Calculating Detonation Properties of C-H-N-O Explosives," Journal of Chemical Physics, 48, pp. 23-25 (1968).

18. Kuo, K. K. and Nydegger, C. C., Journal of Ballistics, 2 (1), pp. 1-25 (1978).

19. Rubin, E. L. and Berstein, S. Z., "Difference Methods for the Inviscid and Viscous Equations of a Compressible Gas," Journal of Computational Physics 2, 178-196 (1967).

20. ...nes, W. F., Nonlinear Partial Differential Equations in Engineering, Academic Press, New York, 1965.

21. Korotkov, A. I., Sulimov, A. A., Obmenin, A. V., Dubovitskii, V. F. and Kurkin, A. I., "Transition from Combustion to Detonation in Porous Explosives," Fizika Goreniya i Vzryva, 5, 315 (1969).

22. Richtmeyer, R. D. and Morton, K. W., Difference Methods for Initial-Value Problems, 2nd Edition, Interscience Publishers, NY, 1967.

23. Kuo,K.K. and Summerfield,M., "High Speed Combustion of Mobile Granular Solid Propellants:Wave Structure and the Equivalent Rankine-Hugoniot Relation," The Combustion Institute,Pittsburgh,PA,(1974).

APPENDIX A

JUMP CONDITIONS FOR TWO-PHASE REACTIVE FLOW

In Section 1.3 (Jump Conditions) of the text the reader was provided with a review of the jump conditions across a shock discontinuity for one-dimensional, <u>one-phase</u> flow with heat addition. This Appendix will outline the development of the jump conditions for one-dimensional, <u>two-phase</u> flow with heat addition. As d scussed in Section 2.3, the heat addition for two-phase flow comes as a release of chemical energy from the ignited propellant particles to the surrounding ga.ei. For a detonation this is assumed to occur in an infinitesimally thin reaction zone.

In order to evaluate the jump conditions for two-phase flow across a steady state combustion wave, the conservation equations (Eqs. 22-27) are first written as conservation equations for the mixture.

Mixture Continuity:

$$\frac{d}{dx} [\phi \rho_g u_g] + \frac{d}{dx} [(1-\phi)\rho_p u_p] = 0 \tag{A.1}$$

Mixture Momentum:

$$\frac{d}{dx} [\phi \rho_g u_g^2 + \phi P_g] + \frac{d}{dx} [(1-\phi)\rho_p u_p^2 + (1-\phi) P_p] = 0 \tag{A.2}$$

Mixture E, ergy:

$$\frac{d}{dx} [\phi \rho_g u_g E_{g_T} + \phi u_g P_g] + \frac{d}{dx} [(1-\phi)\rho_p u_p E_{p_T}$$
$$+ (1-\phi)u_p P_p] = 0 \tag{A.3}$$

As in Secti..... 1.3. the unreacted or "cold" end is denoted by subscript A and the products or "hot" end is denoted by subscript B in the analysis

that follows.

The mixture conservation equations (Eqs. A.1-A.3) are now integrated from the "cold" end to the "hot" end of the bed with the boundary conditions

$$\phi(B) = 1.0$$

$$u_g(A) = u_p(A) = V_A$$

$$u_g(B) = V_B$$

$$\rho_g(B) = \rho_B$$

Integrated Mixture Continuity:

$$\rho_B V_B = \phi_A \rho_{g_A} V_A + (1-\phi_A)\rho_{p_A} V_A \tag{A.4}$$

Integrated Mixture Momentum:

$$P_B + \rho_B V_B^2 = \phi_A [\rho_{g_A} V_A^2 + P_{g_A}]$$

$$+ (1-\phi_A)[\rho_{p_A} V_A^2 + P_{p_A}] \tag{A.5}$$

Integrated Mixture Energy:

$$\left[\rho V (E_{g_T})\right]_B + P_E V_P = \left[\phi \rho_g V (E_{g_T})\right]_A$$

$$+ \left[(1-\phi)\rho_p V(E_{p_T})\right]_A + \left[P_g V\right]_A + \left[(1-\phi)P_p V\right]_A \tag{A.6}$$

At first glance, Equation A.4 to A.6 seem to be easily evaluated knowing the conditions at both ends of the flow. However, as was pointed out by Kuo and Summerfield [23], they are not simple algebraic equations until P_{p_A}, the stress transmitted through the particle phase at location A, is evaluated. This was shown to be obtainable by integrating the momentum equation from the cold end, A, to the location where the particles are no

longer in contact, denoted by subscript C. From this you obtain

$$-P_{p_A} (1-\phi_A) = - \int_A^C \mathcal{D} \, dx + \int_A^C \Gamma \, u_p \, dx$$

$$+ \left[\rho_p \, u_p^2 \, (1-\phi) \right]_C - \left[\rho_p \, V^2 (1-\phi) \right]_A \qquad (A.7)$$

It should be noted that if the flow situation being modeled consists of an infinetly long bed, then the particle stress at location A, P_{p_A}, will also be equal to zero. This is true since pressure disturbances initiated at the combustion zone (i.e., compression of the propellant particles) are propagated through the medium at the speed of sound of the solid, and would therefore take an infinite amount of time to reach location A.

Since all experimental work consists of finite length beds (the numerical model studied in this report was L = 25 cm), a comment on the integration limits of Equation A.7 is appropriate. If the region where particle drag is of significance extends from the combustion wave (C) to the wall condition (A), then the integrals in Equation A.7 must be evaluated after each time increment and hence the particle stress at the wall, P_{p_A}, is changing. However, if the region of significant particle drag is assumed to be only that zone immediately ahead of the combustion zone, then the integrals in Eq. A.7 are always constant and, therefore, P_{p_A} is also constant.

A final comment on the particle stress is that if the time to detonation is less than the time it takes a pressure disturbance to travel through the solid matrix to the rear wall, then the rear wall has not felt the pressure disturbance and hence, $P_{p_A} = 0$.

APPENDIX B

CONSTITUTIVE RELATIONS

As discussed in Chapter 2, a system of nine independent equations is necessary in order to solve for the nine unknown variables describing two-phase flow: ρ_g, ρ_p, u_g, u_p, E_g, E_p, P_g, P_p and ϕ.

Of the three additional equations necessary for the solution, one is the nonideal equation of state for the gas phase as described in the text.

$$\frac{P_g}{RT_g} = 1 + b\rho_g + c\,(b\rho_g)^2 + \ldots \tag{B.1}$$

Values for the constants b and c are discussed in Appendix C.

The second represents an equation of state which relates the solid density to the stress on the particle. (See Ref. 3). This is also mentioned in the text.

$$P_p = ((\frac{\rho_p}{\rho_o})^3 - 1)\,\frac{K_o}{3} \tag{B.2}$$

Finally, the third additional constraint is a relation for the particle phase stress, P_p, as a function of the solids loading and the material bulk modulus, K_o (also see Ref. 3).

As discussed in References 2 and 3, one must also specify functional relations for the following:

a) $\Gamma \equiv$ mass generation rate per unit volume

$$\Gamma = \frac{3}{r_p}\,(1-\phi)\,\rho_p\,\dot{r} \tag{B.3}$$

Here, r_p is the instantaneous particle radius and $\dot{r}$ is the surface burning

rate specified as a function of pressure (and possibly particle temperature).
For all cases run in this study.

$$\dot{r} = b P^n \tag{B.4}$$

where $\dot{r}$ has units of (in/sec), P (psi) and $\underline{b}$ is of the order (1×10^3)
$\dfrac{\text{in/sec}}{(\text{psi})^n}$.

    b) $\mathcal{D} \equiv$ interphase (gas-particle) viscous force (as discussed in the text).

$$\mathcal{D} = \frac{\mu_g}{4r_p^2} \ (u_g - u_p) \ f_{pg} \tag{B.5}$$

where

$$f_{pg} = 5.06 \times 10^5 \ r_p \ Re/u_g^2 \quad (\text{see Eq. 37})$$

    c) $\dot{Q} \equiv$ interphase heat transfer rate

$$\dot{Q} = \frac{3}{r_p} \ (1-\phi) \ h_{pg} \ (T_g - T_p) \tag{B.6}$$

In the analysis carried out here, the heat transfer coefficient was

$$h_{pg} = 0.65 \ [\frac{k_g}{2r_p}] \ [Re]^{0.7} \ (Pr)^{0.33} \tag{B.7}$$

where k_g is the thermal conductivity, Re is the Reynolds number and Pr is
the Prandtl number.

APPENDIX C

NONIDEAL EQUATIONS OF STATE

As described by Jacobs [15], the nonideal equation of state is initially written as a polynomial expansion in gas density.

$$\frac{Pv}{RT} = 1 + x + cx^2 + dx^3 + \ldots \tag{C.1}$$

Here, $x = b\rho = \frac{b}{v}$.

If C_v, the specific heat at a constant volume, is assumed constant over the varying temperatures, as was in the model, Eq. C.1 can be written as:

$$P_v = (\gamma_i - 1) \, E \, f(v) \tag{C.2}$$

In Eq. C.2, γ_i is the specific heat ratio for the ideal gas limit, $\gamma_i = \frac{C_p}{C_v}$, and $f(v)$ is the gas density polynomial expansion.

$$f(v) = 1 + \frac{b}{v} + c\left(\frac{b}{v}\right)^2 + \ldots \tag{C.3}$$

For simplicity the higher order terms are dropped.

The local speed of sound, a, in the detonation state is defined as:

$$a^2 = \frac{P\gamma}{\rho} = \left(\frac{\partial P}{\partial \rho}\right)_s \tag{C.4}$$

Here, γ is the effective specific heat ratio in the detonation state. For detonating explosives γ is typically between two to three. The equality in Equation C.4 is now specified.

$$\gamma \;=\; \frac{\rho}{P}\,\left(\frac{\partial P}{\partial \rho}\right)_s \;=\; \frac{\rho}{P}\,\left(\frac{\partial P}{\partial v}\right)_s\;\left(\frac{\partial v}{\partial \rho}\right)_s \;=\; \frac{\rho}{P}\,\left(\frac{\partial P}{\partial v}\right)_s\left(-\frac{1}{\rho^2}\right)$$

o:

$$\gamma \;=\; \frac{-v}{P}\,\left(\frac{\partial P}{\partial v}\right)_s \tag{C.5}$$

Since $P = P(E, v)$,

$$dP \;=\; \left(\frac{\partial P}{\partial E}\right)\;dE \;-\; \left(\frac{\partial P}{\partial v}\right)\;dv \tag{C.6}$$

and

$$\left(\frac{dP}{dv}\right) \;=\; \frac{\partial P}{\partial E}\Big)_v\;\frac{dE}{dv}\Big)_s \;-\; \frac{\partial P}{\partial v}\Big)_E\,\left(\frac{dv}{dv}\right)_s \tag{C.7}$$

Substituting Eq. C.7 and the constant entropy thermodynamic relation

$$P \;=\; -\frac{\partial E}{\partial v}\Big) \tag{C.8}$$

into Eq. C gives:

$$=\; \frac{-v}{P}\;\;\;\;\;_v\;\;\frac{\partial E}{\partial v}\Big)_s \;+\; \left(\frac{\partial P}{\partial v}\right)_E$$

or

$$\frac{}{\partial E} \tag{C.9}$$

n order to evaluate the second derivative appearing in Eq. C.9 first, the partial of Eq. C.2 with respect to v is taken holding E constant,

$$\frac{\partial}{\partial v}\Big)_E \;=\; \frac{\gamma}{v} \;\;\;\;\; \frac{f'(v)}{} \tag{C.10}$$

and second the part a of Eq. C with respect to E is taken, holding v constant

$$\left(\frac{\partial}{\partial E}\right)_v \;=\; \frac{(\;-1)}{} \tag{C.11}$$

The sum of these in Eq. C.9 now

the form:

$$\gamma = (\gamma_i - 1) \, f(v) + \frac{(\gamma_i - 1) \, E \, f(v)}{Pv} - \frac{(\gamma_i - 1) \, E \, f'(v) v}{Pv} \qquad (C.12)$$

But, since from Eq. C.2

$$\frac{Pv}{(\gamma_i - 1) E} = \frac{1}{f(v)}$$

Eq. C.12 is now:

$$\gamma = (\gamma_i - 1) \, f(v) + 1 - v \, \frac{f'(v)}{f(v)} \qquad (C.13)$$

Knowing approximately what value of γ an explosive exhibits, values of the constant b and c can be fit to equate Eq. C.13.

APPENDIX D

FINITE DIFFERENCING TECHNIQUES

This section will give the reader a more detailed description of the finite differencing scheme referred to in Chapter 3, the Lax-Wendroff center differencing technique.

In order to solve the system of six hyperbolic partial differential equations describing two-phase reactive flow, the Lax-Wendroff scheme presented in Reference 19 for one-phase flow was modified to model two-phase flow. This modification was necessary because of the interactive source-sink terms involved in the governing equations.

The six conservation equations described in Chapter 2 (Eqs. 22 to 27) can be written in vector form as:

$$\frac{\partial U}{\partial t} + \frac{\partial F}{\partial x} = C \tag{D.1}$$

In this notation U, F and C are the vectors

$$U = \begin{bmatrix} \rho_1 \\ \rho_2 \\ \rho_1 u_g \\ \rho_2 u_p \\ \rho_1 E_{g_T} \\ \rho_2 E_{g_T} \end{bmatrix} \qquad F = \begin{bmatrix} \rho_1 u_g \\ \rho_2 u_p \\ (\rho_1 u_g^2 + \phi P_g) \\ (\rho_2 u_p^2 + (1-\phi)P_p) \\ (\rho_1 u_g E_{g_T} + \phi u_g P_g) \\ \rho_2 u_p E_{p_T} + (1-\phi) u_p P_p) \end{bmatrix}$$

$$
C = \begin{bmatrix}
\Gamma \\
-\Gamma \\
\Gamma\, u_p - \mathcal{V} \\
-\Gamma\, u_p + \mathcal{V} \\
\Gamma(E_{CHEM}^{\mathbf{8}} + \dfrac{u_p^2}{2}) - \mathcal{V}\, u_p - \dot{Q} \\
\Gamma(E_{CHEM}^{p} - \dfrac{u_p^2}{2}) + \mathcal{V}\, u_p + \dot{Q}
\end{bmatrix}
$$

The Lax-Wendroff solution, as described by Richtmeyer and Morton [22] begins as a Taylor's series expansion accurate to the second-order.

$$
U_x^{t+\Delta t} = U_x^t + \Delta t \left[\frac{\partial U}{\partial t}\right]_x^t + \frac{1}{2} \angle t^2 \left[\frac{\partial^2 U}{\partial t^2}\right]_x^t \tag{D.2}
$$

In order to make use of Equation D.2, the time derivatives must be replaced by derivatives in space.

By using Equation D.1 and introducing the matrix A, where $A_{ij} = \dfrac{\partial F_i}{\partial U_j}$

$$
\frac{\partial^2 U}{\partial t^2} = \frac{\partial}{\partial t}\left[C - \frac{\partial F}{\partial x}\right] = \frac{\partial C}{\partial t} - \frac{\partial}{\partial x}\left[\frac{\partial F}{\partial t}\right] = \frac{\partial C}{\partial t} - \frac{\partial}{\partial x}\left[A \frac{\partial U}{\partial t}\right] = \frac{\partial C}{\partial t} - \frac{\partial}{\partial x}\left[A \frac{\partial F}{\partial x}\right] \tag{D.3}
$$

Replacing x-derivatives with finite difference quotients (i.e., $\partial F/\partial x = (F_{x+\Delta x} - F_{x-\Delta x})/2\Delta x$), the Lax-Wendroff solution can now be written

$$
U_x^{t+\Delta t} = U_x^t - \frac{\Delta t}{2\Delta x}\left[F_{x+\Delta x}^t - F_{x-\Delta x}^t\right] + \Delta t \cdot C
$$

$$
- \frac{1}{2}\left[\frac{\Delta t}{\Delta x}\right]^2 \left[A_{x+\frac{\Delta x}{2}}^t \left(F_{x+\Delta x}^t - F_x^t\right) - A_{x-\frac{\Delta x}{2}}^t \left(F_x^t - F_{x-\Delta x}^t\right)\right] + \frac{1}{2}\Delta t \cdot C \tag{D.4}
$$

$A^t_{x+\frac{\Delta x}{2}}$ denotes $A\left[\frac{1}{2} U^t_{x+\Delta x} + \frac{1}{2} U^t_x\right]$. For A a constant matrix the Lax-Wendroff

solution takes the form

$$U^{t+\Delta t}_x = U^t_x - \frac{A}{2}\frac{\Delta t}{\Delta x}\left[U^t_{x+\Delta x} - U^t_{x-\Delta x}\right]$$

$$+ \frac{1}{2}\left[A\frac{\Delta t}{\Delta x}\right]^2\left[U^t_{x+\Delta x} - 2U^t_x + U^t_{x-\Delta x}\right] + \frac{3}{2}\Delta t \cdot C \qquad (D.5)$$

Richtmeyer [22] developed a variation of the Lax-Wendroff solution al-

so of second-order accuracy. This method involves two steps and eliminates

the use of the A matrix found in the Taylor's series expansion solution.

Richtmeyer's first step involves computing intermediate values in

time and x-location of U.

Step 1

$$U^{t+\frac{\Delta t}{2}}_{x+\frac{\Delta x}{2}} = \frac{1}{2}\left[U^t_{x+\Delta x} + U^t_x\right] + \frac{t}{2\Delta x}\left[F^t_{x+\Delta x} - F^t_x\right] + \frac{\Delta t}{2}\cdot C^t_x \qquad (D.6)$$

Step 2

$$U^{t+\Delta t}_x = U^t_x + \frac{\Delta t}{\Delta x}\left[F^{t+\frac{\Delta t}{2}}_{x+\frac{\Delta x}{2}} - F^{t+\frac{\Delta t}{2}}_{x-\frac{\Delta x}{2}}\right] + \Delta t \cdot C^t_x \qquad (D.7)$$

The first step (Eq. D.6) is of first-order accuracy. However, the final

step (Eq. D.7) is accurate to the second-order since F quantities of

$\theta(\Delta x)$ are differenced over Δx. For the linear case where F(U) = AU

Equations D.6 and D.7 combine to yield the Lax-Wendroff solution, Equa-

tion D.5.

A two-dimensional (x-t) grid is helpful in understanding how the

Lax-Wendroff differencing scheme can be applied to the numerical solution

of the conservation equations on a digital computer. In Figure D.1 a known

value of the vector U (mass, momentum and energy per unit volume) at a
time $t = t_0$ and located at $x = x_0$ is indicated on the grid by a solid
dot at (x_0, t_0). Locations where the vector U is yet to be solved at
are indicated by open circles. Figures D.2 and D.3 illustrate the
Richtmeyer two-step routine using the x-t grid. For instance, in Figure
D.2 the vector U at $(x_0 - \frac{\Delta x}{2}, t_0 + \frac{\Delta t}{2})$ is solved for by using known values
at two locations (x_0, t_0) and $(x_0 - \Delta x, t_0)$.

In a later paper by Rubin and Berstein [19] it was shown for one-
phase flow that a modified version of Richtmeyer's 2-step method was
more stable in solving the system of equations. The use of half-time
steps was eliminated by averaging F differences at present time, t_0, and
future time, $t_0 + \Delta t$. This is written as

Step 1

$$U^{t+\Delta t}_{\frac{x+\Delta x}{2}} = \frac{U^t_{x+\Delta x} + U^t_x}{2} + \frac{\Delta t}{\Delta x}\left[F^t_{x+\Delta x} - F^t_x\right]$$ (D.8)

Step 2

$$U^{t+\Delta t}_x = U^t_x + \frac{\Delta t}{2\Delta x}\left[\frac{1}{2}\left[F^t_{x+\Delta x} - F^t_{x-\Delta x}\right] + F^{t+\Delta t}_{\frac{x+\Delta x}{2}} - F^{t+\Delta t}_{\frac{x-\Delta x}{2}}\right]$$ (D.9)

This method is illustrated in Figures D.4 and D.5 on the following page.

The following is a summary of the schemes described in this Appendix.
Each will be applied to the gas continuity equation of 1-D, two-phase flow.
Here, Γ represents the gas being generated from the solid phase.

Gas continuity equation

$$\frac{\partial \rho_1}{\partial t} + \frac{\partial \rho_1 u_g}{\partial x} = \Gamma$$ (D.10)
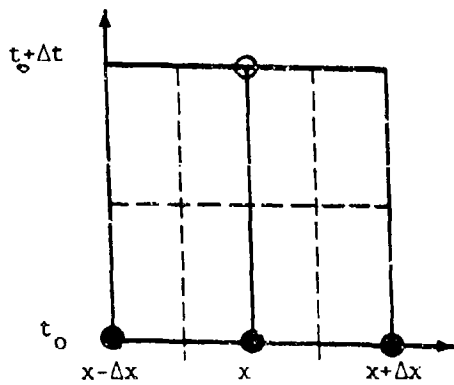
Fig. D.1   Schematic of x-t Grid Used to
Illustrate Finite Differencing
Techniques. Open Circles Indicate
Values Solved for and Black Dots
Represent Known Values.

84

Richtmeyer Two-Step
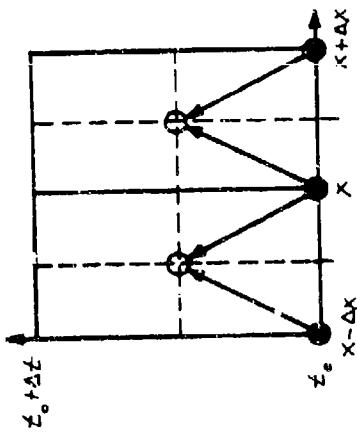
Fig. D.2 Step 1

Fig. D.3 Step 2

85
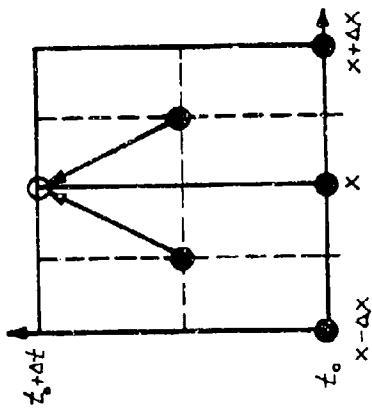
Method of Rubin/Berstein
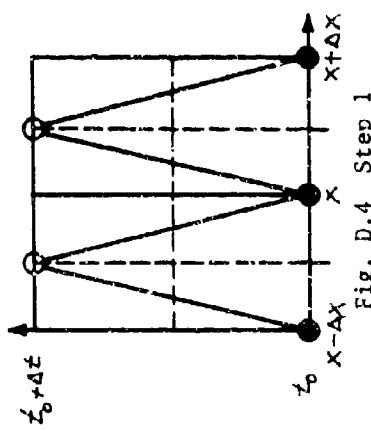
Fig. D.4 Step 1
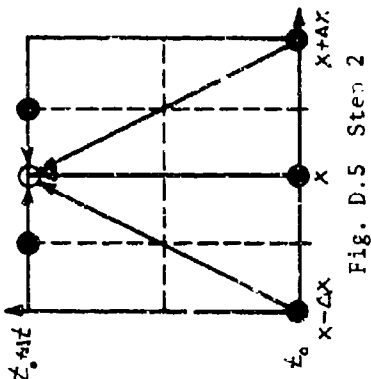
Fig. D.5 Step 2

Richtmeyer 2-step Method

Step 1

$$(\rho_1)_{x+\frac{\Delta x}{2}}^{t+\frac{\Delta t}{2}} = \frac{(\rho_1)_{x+\Delta x}^{t} + (\rho_1)_{x}^{t}}{2} - \frac{\Delta t}{2\Delta x}\left[(\rho_1 u_g)_{x+\Delta x}^{t}\right.$$

$$\left. - (\rho_1 u_g)_{x}^{t}\right] + \Gamma\frac{\Delta t}{2} \qquad (D.11)$$

Step 2

$$(\rho_1)_x^{t+\Delta t} = (\rho_1)_x^{t} - \frac{\Delta t}{\Delta x}\left[(\rho_1 u_g)_{x+\frac{\Delta x}{2}}^{t+\frac{\Delta t}{2}} - (\rho_1 u_g)_{x-\frac{\Delta x}{2}}^{t+\frac{\Delta t}{2}}\right] + \Gamma\frac{\Delta t}{2} \quad (D.12)$$

LW2 - Method of Rubin/Berstein

Step 1

$$(\rho_1)_{x+\frac{\Delta x}{2}}^{t+\Delta t} = \frac{(\rho_1)_{x+\Delta x}^{t} + (\rho_1)_{x}^{t}}{2} - \frac{\Delta t}{\Delta x}\left[(\rho_1 \mu_g)_{x+\Delta x}^{t}\right.$$

$$\left. - (\rho_1 \mu_g)_{x}^{t}\right] + \Gamma \cdot \Delta t \qquad (D.13)$$

Step 2

$$(\rho_1)_x^{t+\Delta t} = (\rho_1)_x^{t} - \frac{\Delta t}{2\Delta x}\left[\frac{(\rho_1 u_g)_{x+\Delta x}^{t} - (\rho_1 u_g)_{x-\Delta x}^{t}}{2}\right.$$

$$\left. + (\rho_1 u_g)_{x+\frac{\Delta x}{2}}^{t+\Delta t} - (\rho_1 u_g)_{x-\frac{\Delta x}{2}}^{t+\Delta t}\right] + \Gamma \cdot \Delta t \qquad (D.14)$$

RECENT AERONAUTICAL AND ASTRONAUTICAL ENGINEERING DEPARTMENT TECHNICAL REPORTS (continued)

Technical Report Number	Title	Author	Journal Publication
AAE 74-10 UILU-ENG 74 0510	An Interior Ballistics Prediction of the M549 Rocket Assisted Projectile	H. Krier S. Shimpi E. Meister	
AAE 75-1 UILU-ENG 75 0501	Dynamically Induced Thermal Stresses in Composite Material, Structural Panels	A. Zak W. Drysdale	
AAE 75-2 UILU-ENG 75 0502	Numerical Analysis of Laminated, Orthotropic Composite Structures	A. R. Zak	
AAE 75-3 UILU-ENG 75 0503	The Characterization and Evaluation of Accidental Explosions	R. A. Strehlow W. E. Baker	NASA CR 134779 (June 1975). Also Progr. Energy & Comb. Sc. (in press).
AAE 75-4 UILU-ENG 75 0504	Program Manual for the Eppler Airfoil Inversion Program	W. G. Thomson	
AAE 75-5 UILU-ENG 75 0505	Design of High Lift Airfoils with a Stratford Distribution by the Eppler Method	W. G. Thomson	
AAE 75-6 UILU-ENG 75 0506	Prediction of Flame Spreading and Pressure Wave Propagation in Propellant Beds	H. Krier	AIAA J. 14: 301-309 (1976)
AAE 75-7 UILU-ENG 75 0507	Vigorous Ignition of Granulated Beds by Blast Impact	H. Krier S. Gokhale	Int. J. Heat-Mass Transfer 19: 915-923 (1976)
AAE 75-8 UILU-ENG 75 0508	Solid Propellant Burning Evaluation with the Dynagun Ballistic Simulator	H. Krier T. G. Nietzke M. J. Adams J. W. Black E. E. Meister	J. Ballistics 1: 103-149 (1976)
AAE 75-9 UILU-ENG 75 0509	Structural Reliability & Minimum Weight Analysis for Combined Random Loads & Strengths	H. H. Hilton	AIAA J. (in press)

RECENT AERONAUTICAL AND ASTRONAUTICAL ENGINEERING DEPARTMENT TECHNICAL REPORTS (Continued)

Technical Report Number	Title	Author	Journal Publication
AAE 75-10 UILU-ENG 75 0510	Linear Viscoelastic Analysis with Random Material Properties	H. H. Hilton J. Hsu J. S. Kirby	
AAE 76-1 UILU-ENG 76 0501	Two Degree of Freedom Flutter of Linear Visco-elastic Wings in Two Dimensional Flow	C. F. Vail H. H. Hilton	In press AIAA J.
AAE 76-2 UILU-ENG 76 0502	An Error Analysis of Computerized Aircraft Synthesis	V. V. Volodin H. H. Hilton	In press J. of Aircraft
AAE 76-3 UILU-ENG 76 0503	Reactive Two-Phase Flow Models Applied to the Prediction of Detonation Transition in Granu-lated Propellant	H. Krier M. Dimitstein S. S. Gokhale	AIAA J. 16: 177-183 (1978)
AAE 76-4 UILU-ENG 76 0504	Transient Temperature Response of Charring Composite Slabs	J. E. Prussing H. Krier	Int'l J. Heat Mass Transfer, 21: 519-522 (1978)
AAE 76-5 UILU-ENG 76 0505	Nonlinear Response of Laminated Composite Material Cylindrical Shells	A. R. Zak J. N. Craddock	
AAE 76-6 UILU-ENG 76 0506	An Investigation of Blast Waves Generated from Non-Ideal Energy Sources	A. A. Adamczyk	
AAE 77-1 UILU-ENG 77 0501	Nonlinear Dynamic Analysis of Flat Laminated Plates by the Finite Element Method	A. R. Zak	
AAE 77-2 UILU-ENG 77 0502	An Investigation of Blast Waves Generated by Constant Velocity Flames	R. T. Luckritz	
AAE 77-3 UILU-ENG 77 0503	On the Blast Waves Produced by Constant Velocity Combustion Waves	R. A. Strehlow R. D. Luckritz	
AAE 77-4 UILU-ENG 77 0504	Direct Initiation of Detonation by Non-Ideal Blast Waves	R. J. Cesarone	
AAE 77-5 UILU-ENG 77 0505	The Blast Wave Generated by Constant Velocity Flames	S. A. Shimpi R. A. Strehlow	

RECENT AERONAUTICAL AND ASTRONAUTICAL ENGINEERING DEPARTMENT TECHNICAL REPORTS (Continued)

Technical Report Number	Title	Author	Journal Publication
AAE 77-6 UILU-ENG 77 0506	Exploratory Studies of Flame and Explosion Quenching	R. A. Strehlow L. C. Sorenson L. D. Savage H. Krier	
AAE 77-7 UILU-ENG 77 0507	The Trajectory of a Liquid Droplet Injected Into the Wake of an Aircraft in Ground Effect	M. B. Bragg	
AAE 77-8 UILU-ENG 77 0508	Comparison of Viscoelastic and Structural Damping in Flutter	H. H. Hilton	
AAE 77-9 UILU-ENG 77 0509	The Blast Wave Generated by Constant Velocity Flames	R. A. Strehlow R. T. Luckritz A. A. Adamczyk S. Shimpi	
AAE 77-10 UILU-ENG 77 0510	Wind Energy: History, Economics, and the Vertical Wind Turbine	T. R. Richards	
AAE 77-11 UILU-ENG 77 0511	Final Report: Low Speed Airfoil Study	A. I. Ormsbee	
AAE 77-12 UILU-ENG 77 0512	Final Report: Propeller Study, Part I, Introduction and Overview	A. I. Ormsbee	
AAE 77-13 UILU-ENG 77 0513	Final Report: Propeller Study, Part II, The Design of Propellers for Minimum Noise	C. J. Woan	
AAE 77-14 UILU-ENG 77 0514	Final Report: Propeller Study, Part III, Experimental Determination of Thrust & Torque on the YO-3A Aircraft	S. A. Siddiqi K. R. Sivier A. I. Ormsbee	
AAE 77-15 UILU-ENG 77 0515	Direct Initiation of Detonation	R. A. Strehlow H. O. Barthel	

RECENT AERONAUTICAL AND ASTRONAUTICAL ENGINEERING DEPARTMENT TECHNICAL REPORTS (Continued)

Technical Report Number	Title	Author	Journal Publication
AAE 77-16 UILU-ENG 77 0516	The Effects of Energy Distribution Rates and Density Distribution on Blast Wave Structure	R. A. Strehlow L. H. Sentman	17th Combustion Symposium: In Press
AAE 77-17 UILU ENG 77 0517	Modeling of Convective Mode Combustion Through Granulated Propellant to Predict Transition to Detonation	H. Krier J. A. Kezerle	
AAE 78-1 UILU ENG 78 0501	Unsteady Internal Boundary Layer Flows with Application to Gun Barrel Heat Transfer and Erosion	M. J. Adams H. Krier	
AAE 78-2 UILU ENG 78 0502	Extracting Burning Rates for Multiperforated Propellant from Closed Bomb Testing	H. Krier	
AAE 78-3 UILU ENG 78 0503	Lean Limit Flammability Study of Methane-Air Mixtures in a Square Flammability Tube	J. Jarosinski R. A. Strehlow	
AAE 78-4 UILU ENG 78 0504	Interim Technical Report AFOSR 77-3336: "An Investigation of the Ignition Delay Times For Propylene Oxide-Oxygen-Nitrogen Mixtures"	E. E. Meister	
AAE 78-5 UILU ENG 78 0505	Final Report: A Distribution Model for the Aerial Application of Granular Agricultural Particles	S. T. Ferrandes A. I. Ormsbee	
AAE 78-6 UILU ENG 78 0506	The Thermal Structure of a Methane-Air Flame Propagating in a Square Flammability Tube	J. Jarosinski R. A. Strehlow	
AAE 78-7 UILU ENG 78 0507	The Effects of Energy Distribution Rates and Density Distribution on Blast Wave Structure	R. A. Strehlow L. H. Sentman	
AAE 78-8 UILU ENG 78 0508	The Effect of a Zero G Environment on Flammability Limits as Determined Using a Standard Flammability Tube Apparatus	R. A. Strehlow D. L. Reuss	

4

RECENT AERONAUTICAL AND ASTRONAUTICAL ENGINEERING DEPARTMENT TECHNICAL REPORTS (Continued)

Technical Report Number	Title	Author	Journal Publication
AAE 79-1 UILU-ENG 79 0501	An Approximate Finite Element Method of Stress Analysis of Non-Axisymmetric Bodies with Elastic-Plastic Material	J. N. Craddock A. R. Zak	
AAE 79-2 UILU-ENG 79 0502	Stability of Bridge Motion in Turbulent Winds	Y. K. Lin S. T. Ariaratnam	
AAE 79-3 UILU ENG 79 0503	Rotor Blade Dynamics in Hovering Flights	C.Y.R. Hong	
AAE 79-4 UILU ENG 79 0504	Finite Element Analysis of A Dynamically Loaded Flat Laminated Plate	D. W. Pillasch A. R. Zak	
AAE 79-5 UILU ENG 79 0505	An Efficient Rotational Nonequilibrium Model of a CW Chemical Laser	L. H. Sentman	
AAE 79-6 UILU ENG 79 0506	Column Response to Vertical-Horizontal Earthquakes	Y. K. Lin T. Y. Shih	
AAE 79-7 UILU ENG 79 0507	Users Guide for Programs MNORO & AFOPTMNORO	L. H. Sentman	
AAE 79-8 UILU ENG 79 0508	The Blast Wave from Deflagrative Explosions, an Acoustic Approach	R. A. Strehlow	
AAE 80-1 UILU ENG 80 0501	Gas Flow Resistance Measurements Through Packed Beds at High Reynolds Numbers	S. F. Wilcox H. Krier	
AAE 80-2 UILU ENG 80 0502	Fluid Mechanical Processes of Deflagration to Detonation Transition in Beds of Porous Reactive Solids	S. Hoffman H. Krier	
AAE 80-3 UILU ENG 80 0503	Dynamic Analysis of Orthotropic, Layered Plates Subject to Explosive Loading	D. W. Pillasch A. R. Zak	

RECENT AERONAUTICAL AND ASTRONAUTICAL ENGINEERING DEPARTMENT TECHNICAL REPORTS (Continued)

Technical Report Number	Title	Author	Journal Publication
AAE 81-1 UILU ENG 81 0501	Shock Development and Transition to Detonation Initiated by Burning in Porous Propellant Beds	P. B. Butler H. Krier	